

Article

A Study on the Influence of Electrical Discharges on the Formation of White Etching Cracks in Oil-Lubricated Rolling Contacts and Their Detection Using Electrostatic Sensing Technique

Kamran Esmaeili ¹, Ling Wang ^{1,*} , Terry J. Harvey ¹ , Neil M. White ² and Walter Holweger ¹ 

¹ National Centre for Advanced Tribology at Southampton (nCATS), Faculty of Engineering and Physical Sciences, University of Southampton, Southampton SO17 1BJ, UK

² Electronics and Computer Science, Faculty of Engineering and Physical Sciences, University of Southampton, Southampton SO17 1BJ, UK

* Correspondence: ling.wang@soton.ac.uk; Tel.: +44-(0)-2380-595076

Abstract: In bearing applications, the presence of stray and parasitic currents in combination with lubricants has been studied for almost a century and has been found to cause fluting and corrugation damages under high current densities. However, recent research has suggested that at low current densities ($<1 \text{ mA/mm}^2$) under specific operating conditions, electrical discharges can substantially reduce bearing life due to the formation of white etching cracks (WECs). To date, limited studies have investigated the critical operating and electrical conditions for WEC formation and demonstrated effective fault detection techniques. This study uses a novel monitoring technique known as the electrostatic sensing technique to detect, monitor and characterise electrical discharges in an oil-lubricated steel–steel rolling contact on a TE74 twin-roller machine. The findings demonstrate that WECs can be formed under the influence of electrical discharges in less than 50 h, and the electrostatic sensors are effective for the early detection of critical electrical discharges related to WEC-induced failures.



Citation: Esmaeili, K.; Wang, L.; Harvey, T.J.; White, N.M.; Holweger, W. A Study on the Influence of Electrical Discharges on the Formation of White Etching Cracks in Oil-Lubricated Rolling Contacts and Their Detection Using Electrostatic Sensing Technique.

Lubricants **2023**, *11*, 164. <https://doi.org/10.3390/lubricants11040164>

Received: 11 February 2023

Revised: 24 March 2023

Accepted: 30 March 2023

Published: 3 April 2023



Copyright: © 2023 by the authors. Licensee MDPI, Basel, Switzerland. This article is an open access article distributed under the terms and conditions of the Creative Commons Attribution (CC BY) license (<https://creativecommons.org/licenses/by/4.0/>).

Keywords: electrostatic sensor; voltage measurement technique; electrical discharges; WEC formation; quantification algorithm; detection and diagnosis

1. Introduction

Since the beginning of the 20th century, researchers have studied the presence of electrical current in industrial machinery and its detrimental influence on machine longevity [1–4]. The presence of electrical current is particularly critical in the application of rolling element bearings in conjunction with lubricants facilitating electrical discharges between contacting surfaces [5].

Early research has focussed on failure modes such as electrical pitting, frosting, fluting and corrugation [6], which were all caused by the presence of strong electrical currents [7]. Busse et al. [8] analysed how current affected bearing lifespan and developed a theoretical model. It was suggested that the primary governing factor is the level of current density that determines the life of bearings, operating under normal conditions. It was proposed that current densities below 400 mA/mm^2 can be considered as “safe”, as the bearing life exceeds 100,000 h (typical bearing life for industrial applications is estimated to be 20,000–40,000 h) [8].

Recent research, however, has shown that bearings can experience a significant reduction in the expected L_{10} life (approximately 5–10%) due to axial cracking or spalling initiated by white etching crack (WEC) formation [9–14] even at current densities below 1 mA/mm^2 and often in the presence of a critical lubricant. WECs are networks of cracks

formed in the subsurface of steel bearings and are accompanied by transformed ultra-fine nano-recrystallised microstructure features [15–20].

Loos et al. [11] investigated the electrical behaviour of bearing contact as a function of electric current and found that at an operating temperature of 100 °C, maximal contact pressure of 2–2.4 GPa, and operating in the full-lubrication regime, the electrical current level of 25–60 $\mu\text{A}/\text{mm}^2$ is the critical current level for the formation of WECs. Zuercher [21] explored the operating and electrical conditions and found that WECs can be created in rolling element bearings whilst operating at a temperature greater than 90 °C, maximal contact pressure of 2.3–3.2 GPa, operating in the full-lubrication regime and current density of 25–200 $\mu\text{A}/\text{mm}^2$. According to the findings of these two studies [9,11,21,22], bearing contacts exhibit the highest electrical resistance and subsequently electrical discharges at these current density levels.

Loos et al. [11] suggested that these high-magnitude electrical discharges are caused by currents combined with lubricants, leading to the decomposition of lubricant molecules. This can subsequently facilitate chemical reactions resulting in the creation of hydrogen cations, which can weaken microstructure and lead to the formation of WECs. Holweger et al. [23], however, argued that the underlying process for WEC formation is the thermal effect, induced by electrical discharges and material inhomogeneities, such as carbides or inclusions. The thermal effect was suggested to lead to local thermal stress and strain which subsequently drive atoms such as carbon, chromium and silicon to diffuse and form WEAs and WECs [24].

However, currently, the main drivers influencing the formation of WECs, including electrical discharges and their critical levels, are still unknown. The authors' earlier research [25] investigated the electrical discharges at a current density as low as 25–300 $\mu\text{A}/\text{mm}^2$ and demonstrated that electrical discharges in terms of frequency and magnitude are influenced by supply voltage (and current) and operating conditions including oil temperature, speed and contact pressure. It was shown that individual electrical discharge events can be detected, characterised and tracked during the course of testing using a novel monitoring technique known as electrostatic (ES) sensing and quantified by an algorithm developed by the authors. This study uses a TE74 twin-roller test rig, ES sensing technology and the quantification algorithm to evaluate the following:

- i. Critical operating conditions for WEC formation;
- ii. Influence of operating parameters on electrical discharges;
- iii. Differences in electrical discharges during WEC and non-WEC tests;
- iv. The early diagnosis of WEC failure using sensing techniques.

All the definitions of abbreviations in this paper can be found in Table 1:

Table 1. Abbreviations and definitions.

Abbreviations	Definitions
ES	Electrostatic
IQR	Interquartile range
LOM	Light optical microscopy
PAO	Polyalphaolefin
PMMA	Polymethylmethacrylate
RCF	Rolling contact fatigue
SRR	Slide-to-roll ratio
VADC	Voltage across the discs' contact
WEC	White etching crack

2. Experimental Details

The materials, procedures and test configuration used in this study are described in the section that follows. Sections 2.1–2.6 are paraphrased from the methodology section of the authors' prior research [25].

2.1. The Test Rig and Samples

Experiments investigating rolling contact fatigue (RCF) under oil lubrication conditions were carried out using a Phoenix Tribology Ltd. TE74 twin-roller machine. The test apparatus employed a pneumatic system to apply a radial load of up to 12 kN on two discs loaded against each other (see Figure 1). The lubricant was supplied to the discs through an inlet port, while excess oil was collected from an oil sump and directed to a storage tank. The temperature of the lubricant within the tank could be varied up to a maximum of 150 °C. The experimental setup was equipped with three K-type thermocouples to monitor the lubricant temperature at the inlet and outlet ports, as well as inside the tank. The electric motor driving the bottom shaft could achieve a maximum speed of 3000 rpm, while the top motor could attain a speed of up to 6000 rpm. The bottom disc was a crowned disc with a transverse diameter of 100 mm and a diameter of 52 mm, while the top disc was flat and had a diameter of 26 mm (please refer to Figure 1 for a schematic representation of the experimental setup).

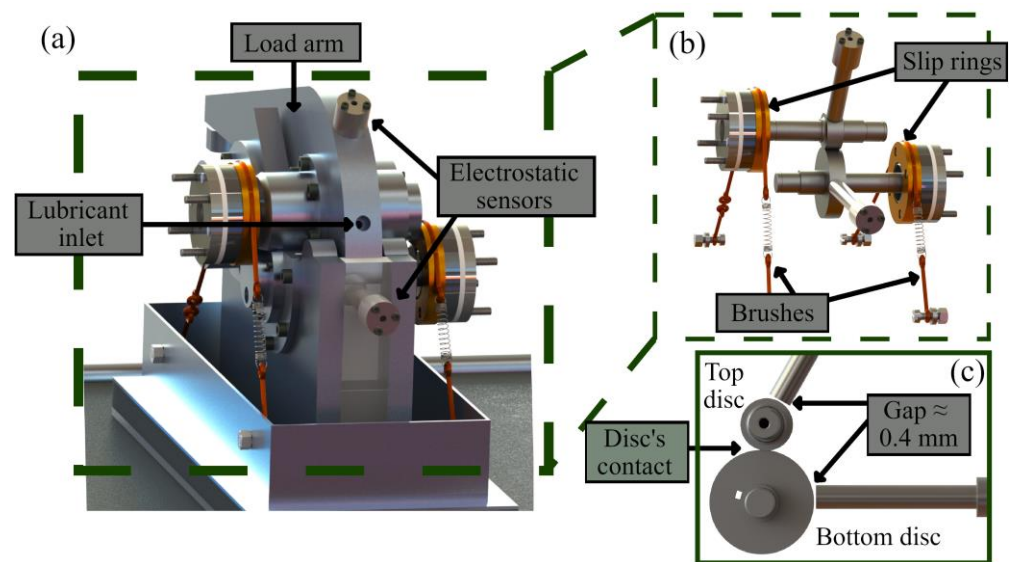


Figure 1. Three-dimensional models of the TE74 twin-roller machine used in the experiments. The first model (a) illustrates the radial load applied by a load arm, along with brushes/slip rings that allow for proper electrical contacts with the rotating parts. The second model (b) depicts the top and bottom discs, and the locations of two ES sensors. Lastly, the third model (c) shows a cross-sectional view of the gap between the ES sensors and the discs, which is approximately 0.4 mm, as well as the contact area of the discs. A keyhole for the larger disc is also visible in this model.

2.2. Electrical Input and Setup

In order to create a voltage difference between the top and bottom discs, a DC power supply was employed, as depicted in Figure 2. To maintain low electrical noise, brushes and slip rings were incorporated to ensure reliable proper electrical connections to the shafts. The circuit was equipped with a 50 k Ω resistor that functioned to restrict the maximum current flow in the system. For instance, at a supply voltage of 15 V, the maximum current in the circuit was limited to 300 μ A. As current flowed from the bottom disc to the top disc, the top disc was designated as the cathodic disc.

2.3. Sensors and Data Acquisition Details

In this experimental investigation, two electrostatic (ES) sensors were employed to study the localised charges linked with the charging and discharging occurrences on the discs. The diameter of the sensor faces was 6 mm, and they were positioned at a distance of roughly 0.4 mm from the disc surfaces, as illustrated in Figure 1b,c. The upper ES sensor

was equipped with a plastic cover to prevent electrical contact with the load arm, whereas the lower ES sensor was affixed to a plastic material and did not require such a cover.

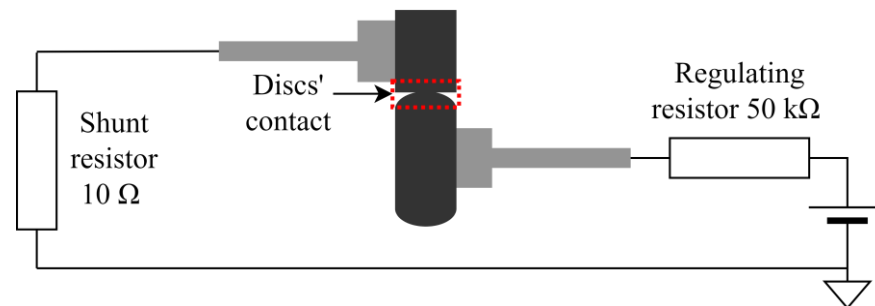


Figure 2. A diagram representing the electrical circuit utilised in the TE74 test apparatus to create a voltage difference across the discs' contact.

To ensure the appropriate insulation and wiring of the ES sensors, a multimeter was used to examine the electrical isolation of the sensor face and shield, as well as the outer body. The output signals from the ES sensors were transformed into voltage signals using a charge amplifier of type Brüel & Kjær 2635. The transducer sensitivity was set to 0.5 pC/V, which represents the conversion rate for electrical charge produced per unit of electrical voltage. The high-pass filter was set to 0.2 Hz to avoid the loss of any low-frequency signals.

The PicoScope 4424 was utilised to capture the voltage between the two discs and the outputs of the two ES sensors, at a sampling rate of 5 MHz for 1 s at 20 s intervals throughout the testing period. Additionally, the current in the circuit, measured by the voltage across the shunt resistor, and supply voltage were recorded using a separate data acquisition device, at 10 kHz for 1 s at an interval of 20 s during the testing period. The test rig software continuously recorded rotational speed (of both discs), radial load and temperatures (of lubricant inlet, outlet and tank) at a rate of 1 Hz.

2.4. Properties of the Material

The test rollers were machined using a bearing steel bar of SAE 52100, and then heat treated according to S133100-1. The heat treatment process comprised austenitisation at a temperature of 850 °C for 30 min, quenching in an oil bath and annealing at 230 °C for 2 h. Tables 2 and 3 exhibit the chemical composition and mechanical properties of the conventional SAE 52100 bearing alloy steel, respectively.

Table 2. Chemical composition of SAE 52100 alloy steel [26].

Element	Content (%)
Iron, Fe	96.5–97.32
Chromium, Cr	1.35–1.60
Carbon, C	0.93–1.05
Manganese, Mn	0.25–0.45
Silicon, Si	0.15–0.35
Sulfur, S	≤0.015
Phosphorous, P	≤0.025

2.5. Lubricant and Additive Packages

Previous research has concentrated on investigating lubricants that lead to the formation of WECs and have identified a lubricant named WW1362 as the most severe lubricant causing WEC formation [27]. This lubricant contains polyalphaolefin (PAO) with a viscosity of 46 mm²/s at 40 °C as the base oil, 5% polymethylmethacrylate (PMMA) as a viscosity index improver, and a mixture of primary and secondary zinc dithiophosphate (2%). The characteristics of WW1362 lubricant are presented in Table 4.

Table 3. Mechanical properties of SAE 52100 alloy steel [26].

Properties	Metric
Bulk modulus	140 GPa
Shear modulus	80 GPa
Elastic modulus	210 GPa
Poisson's ratio	0.27–0.30
Density	7.81 g/cm ³
Melting point	1424 °C
Hardness, Rockwell C scale (HRC)	Retained austenite 10–12% 61.5

Table 4. The physical properties of the WW1362 lubricant.

Properties	Value	Unit
Density at 15 °C	883	kg/m ³
Dielectric strength	26.4	kV/mm
Kinematic viscosity at 40 °C	60.34	mm ² /s
Kinematic viscosity at 100 °C	8.69	mm ² /s

2.6. Roughness Measurement of the Disc Samples

Disc surface roughness was evaluated prior to the testing using a Talysurf 120 L laser profilometer from Taylor Hobson in accordance with the ISO 4288-1996 standard. The stylus of the profilometer was diamond-tipped with a radius of 2 µm and a vertical resolution of 0.25 nm. Since the discs were polished in the rolling direction, they exhibited a periodic pattern, and therefore, a spacing distance (RSm) was utilised with an appropriate cut-off value. According to the standard, the evaluation length should be at least 5 times the cut-off value to provide at least 5 evaluation windows for precise measurement of the roughness. For all the analyses conducted in this study, the evaluation length was held constant at 9 mm. To obtain an accurate estimate of the surface roughness, four measurements were conducted on each disc, equally spaced around the disc.

2.7. Evaluation of Minimum Film Thickness and Lubricant Regime

For all the performed tests, the measurement of the slave (top disc) and master (bottom disc) shaft speeds, the lubricant inlet temperature and the radial load, together with the initial roughness of the discs, allowed for the calculation of minimum film thickness and lambda for the duration of the tests. Minimum film thickness defines the minimum distance between the two discs in motion, and its thickness depends on factors such as the viscosity of the lubricant, the contact pressure between the surfaces and the temperature. The lambda ratio is a parameter used to analyse contact friction and wear and is defined as the ratio of the minimum film thickness to the combined roughness of the surfaces in motion. The minimum film thickness and lambda are calculated using the equations detailed in Appendix A.

2.8. Metallographic Analysis to Examine Surface and Subsurface Failures

At the end of each test, the discs were thoroughly analysed for any surface or subsurface damages. After each test, the rig was disassembled, and the samples were removed for further inspection. If damage was found, the disc was cut adjacent to the wear track and the damage to enable further processing (see Figures 3b and 4b). In case of no damage, the disc was cut adjacent to the wear track for both edges.

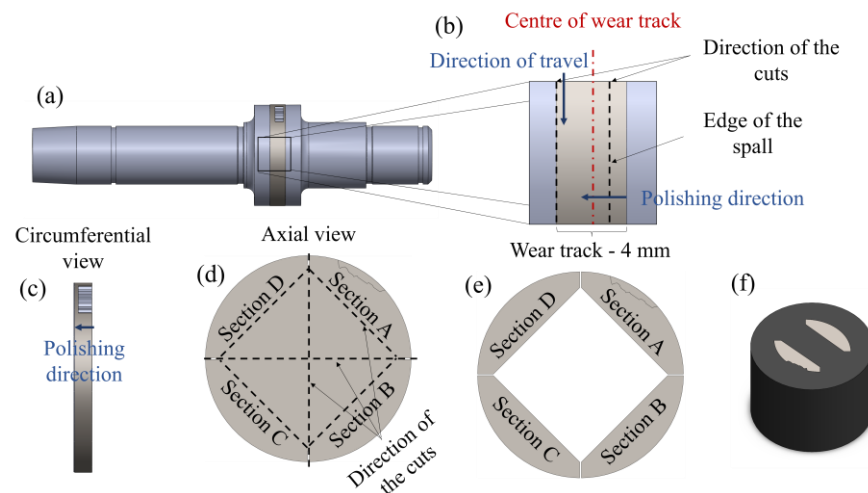


Figure 3. Material preparation and mounting for the 26 mm disc, showing the wear track in (a), cutting and polishing directions in (b,c); and sample preparation for surface and subsurface investigations in (d–f).

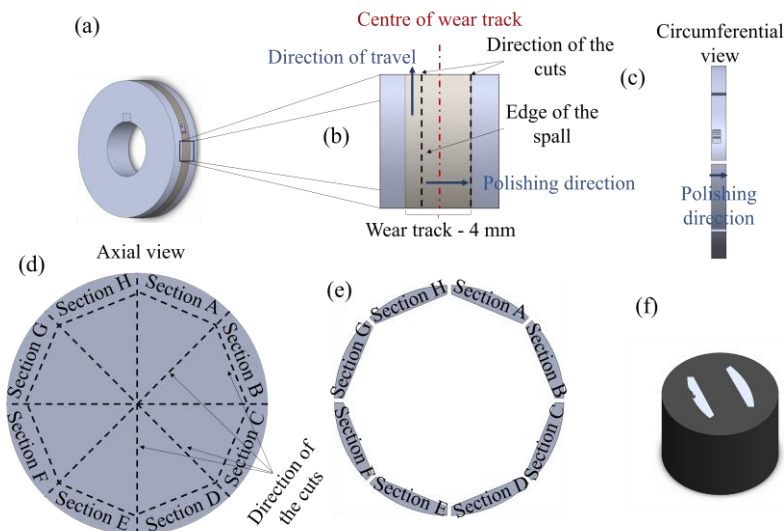


Figure 4. Material preparation and mounting for the 52 mm disc, with (a,b) showing the wear track and the direction of cutting, (c) representing the polishing direction, and (d–f), demonstrating the sample preparation for surface and subsurface investigations.

Following this stage, the discs were then cut into four and eight equal pieces for the 26 and 52 mm discs, respectively, as shown in Figures 3d and 4d. The inner sections of the samples were removed to allow for an accelerated grinding process and ease of specimen inspection under light optical microscopy (LOM). Each section was carefully examined under LOM to identify any features that would aid in selecting the sections for further analysis.

Following the inspection, the selected samples were then thoroughly cleaned in an ultrasonic bath and hot-mounted using a conductive Bakelite resin. The samples were then ground and polished to achieve a mirror finish and etched with nital solution.

Following the etching process, the samples were observed under LOM to identify any features such as WECs in the subsurface of the samples. The grinding, polishing, etching and LOM inspection stages were repeated with an approximate grinding interval of 250 μm until a desired feature was observed or $\frac{3}{4}$ of the wear track was examined.

2.9. Test Matrix

Previous studies [11,21] focussed on the influence of electrical discharges on WEC formation have shown that an electric current of 25–70 μA results in the highest voltage

across the disc contact and the formation of WECs. In this study, it was decided to limit the maximum electric current in the circuit to below 200 μA by limiting the maximum voltage supplied to 10 V when a regulating resistor of 50 k Ω is used.

The master shaft rotational speed was kept constant at 3000 rpm to allow for the maximum stress cycles and lower running time. According to the literature, WECs form under maximal contact pressure of 1.6–2.4 GPa [11,21], and an increase in maximal contact pressure would typically reduce the time to failure. The maximal contact pressure in this study was kept constant at 2.5 GPa to accelerate WEC formation without inducing other severe damages. For a WEC test, the critical temperature of the bearings has been reported to be between 80 and 100 $^{\circ}\text{C}$ [9–11,21,28]; thus, this range was applied in this study. Table 5 shows details of the 12 tests performed on the TE74 twin-roller test rig with three main controlling parameters of (i) slide-to-roll ratio (SRR), (ii) lubricant inlet temperature and (iii) discs' surface roughness [29].

Table 5. Details of the tests; master speed and load were kept constant at 3000 rpm and 3340 N, respectively, resulting in maximal contact pressure of 2.5 GPa and contact area of 2 mm². The highlighted cells indicate the main parameters that were changed between the tests.

Test Index	SRR (%)	Supply Voltage (V)	Lubricant Inlet Temperature ($^{\circ}\text{C}$)	The Roughness of the Top Disc (μm)	The Roughness of the Bottom Disc (μm)	Minimum Film Thickness (μm)	Lambda
1	No	10	75	0.025	0.029	0.268	7
2	5	10	80	0.025	0.029	0.249	6.5
3	5	10	100	0.025	0.029	0.153	4
4	15	10	100	0.025	0.029	0.153	4
5	15	10	95	0.208	0.112	0.189	0.8
6	15	10	100	0.094	0.385	0.159	0.4
7	15	0	100	0.087	0.142	0.133	0.8
8	15	10	100	0.071	0.102	0.186	1.5
9	15	10	100	0.199	0.110	0.182	0.8
10	15	10	100	0.306	0.200	0.146	0.4
11	15	10	100	0.199	0.110	0.182	0.8
12	No	10	95	0.199	0.110	0.182	0.8

Initial lubricant film thickness, contact area, maximal contact pressure and lambda were calculated for the tests according to Appendix A and are presented in Table 5.

Tests 1–4 were performed to investigate the influence of SRR (0–15%) and lubricant inlet temperature (75–100 $^{\circ}\text{C}$) on the electrical discharges and the formation of WECs under full-lubrication conditions. Tests 5, 6 and 8–11 were performed on roughened discs whilst the SRR and temperature were kept constant, except Test 5 with 5 $^{\circ}\text{C}$ lower temperature, to study the influence of lambda on the electrical discharges and WEC formation. Test 7 was performed under conditions similar to those of Test 5 (see lambda values) without any voltages supplied to the contact in order to evaluate the influence of voltage on WEC formation. Test 12 was conducted under conditions similar to those of Test 5 to investigate the influence of SRR.

3. Results

3.1. The Outcome of the Tests

3.1.1. Surface Analysis

Immediately after the tests (terminated either automatically due to failure or manually when the pre-determined duration was reached), the samples were processed for any indication of surface damage or features. As the 26 mm roller experienced nearly twice the number of rolling cycles as the 52 mm disc and is the cathodic end, it is expected to fail more rapidly [9,10,21,22,25]. Although the analysis was performed for both 52 mm and 26 mm discs, only the results from the analysis on 26 mm discs are presented here. The details of the tests including the median lubricant inlet temperature, the median lambda

(based on the initial roughness values), the running time and cycles and the stop types are detailed in Table 6.

Table 6. The surface and subsurface analysis of the samples; master speed and load were kept constant at 3000 rpm and 3340 N, respectively, resulting in maximal contact pressure of 2.5 GPa and contact area of 2 mm². The highlighted cells indicate the main parameters that were changed between the tests.

Test Index	SRR (%)	Median Lubricant Inlet Temperature (°C)	Supply Voltage (V)	Minimum Film Thickness (µm)	Median Lambda	Duration (Hours)	Cycles (Millions)	Stop Type	Outcome
1	No	73.3	10	0.278	7.25	335.77	60.44	Manual	No damage
2	5	76.8	10	0.253	6.6	305.38	54.97	Manual	No damage
3	5	98.5	10	0.165	4.31	285.08	51.31	Manual	No damage
4	15	97.3	10	0.163	4.27	305.86	55.05	Manual	No damage
5	15	92.2	10	0.180	0.76	39.82	7.17	Automatic	Spall, WEC networks in 26 mm disc
6	15	98.7	10	0.159	0.4	2.75	0.50	Automatic	Severe pitting, surface failure of 26 mm disc
7	15	98.2	0	0.158	0.95	239.71	43.15	Manual	No damage
8	15	96.0	10	0.167	1.34	35.69	6.42	Manual	No damage
9	15	97.5	10	0.161	0.71	45.72	8.23	Manual	Pitting, WEC networks in 26 mm disc
10	15	98.2	10	0.161	0.44	14.52	2.61	Automatic	Severe pitting, surface failure of 26 mm disc
11	15	97.7	10	0.161	0.71	14.93	2.70	Manual	No damage
12	No	92.7	10	0.186	0.82	114.85	20.67	Manual	No damage

The wear track observed in Test 2 exhibited colourful parallel patterns after continuous operation for over 300 h, as depicted in Figure 5. These patterns were attributed to the experienced level of friction and heat and may indicate the formation of a tribofilm [30]. Increasing the temperature to 100 °C in Test 3 increased the experienced friction and heat, resulting in wider discolouration and tribofilm formation covering the full width of the wear track, with specific colours indicating different compositions [31,32]. Increasing the SRR to 15% in Test 4 influenced the discolouration as well as composition of the tribofilm, resulting in brighter colours.

In Test 5, the roughness values were increased in order to lower lambda to 0.76, and the test failed automatically due to a spall at approximately 40 h. The surface displays the same discolouration appearing in dark red and covering the full width of the wear track. It appears that the discolouration and the composition of the tribofilm are consistent across the wear track. Test 6, under a substantially lower lambda value, failed to reach 3 h of operation and failed with pits appearing on the surface (see Figure 5e). For this test, the discolouration appears to be of a faint nature, perhaps due to the short duration of the test.

The discolouration in Test 7 is more pronounced than that in any other tests, mainly due to the experienced heat and friction for a prolonged period. This may have led to the formation of a tribofilm fully covering the wear track. This is shown as dark red features on the surface in Figure 5f. Test 7 was performed under approximately the same operating conditions as Test 5, but without any supply voltage, and lasted for nearly 240 h without any surface damage.

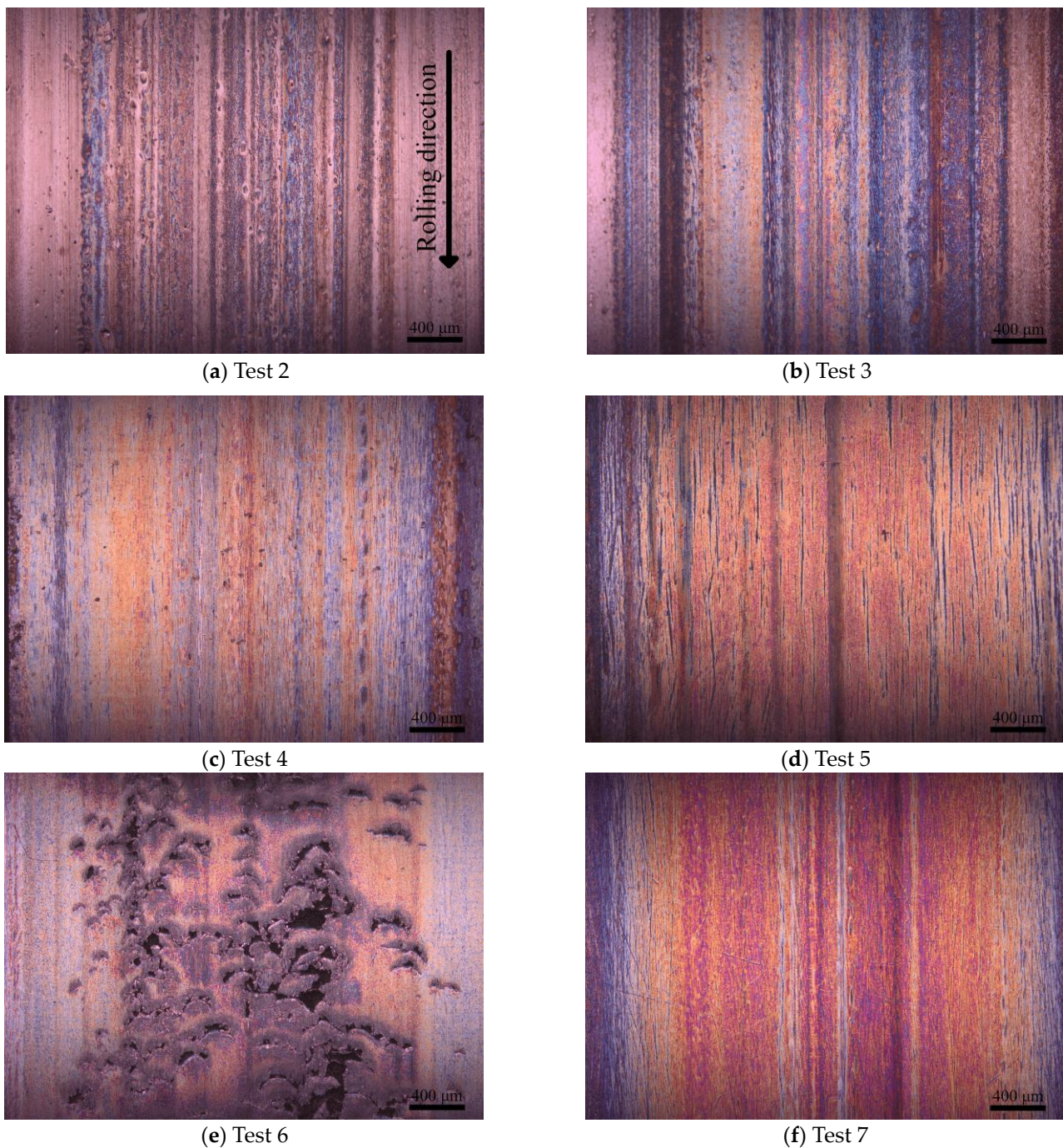


Figure 5. Surface images of the 26 mm discs for (a) Test 2, (b) Test 3, (c) Test 4, (d) Test 5, (e) Test 6 and (f) Test 7. The arrow indicates the rolling direction for all the images, and the scale bar at the bottom right of the images shows 400 μm .

Test 8 was performed under operating conditions similar to those of Test 5, but with a lambda of 1.34 (instead of 0.76). As shown in Figure 6a, no surface damage was observed for Test 8, and it was manually terminated after 36 h. Similar to Test 6, the surface shows bright red colours. Test 9 was conducted at a lambda value of 0.71 and was terminated manually after approximately 46 h. Nevertheless, upon conducting surface analysis of the specimens, it was observed that pits had formed on the surface. This can be visually corroborated through Figures 6b and 7g. Additionally, red features similar to those identified in Test 5 were also noted.

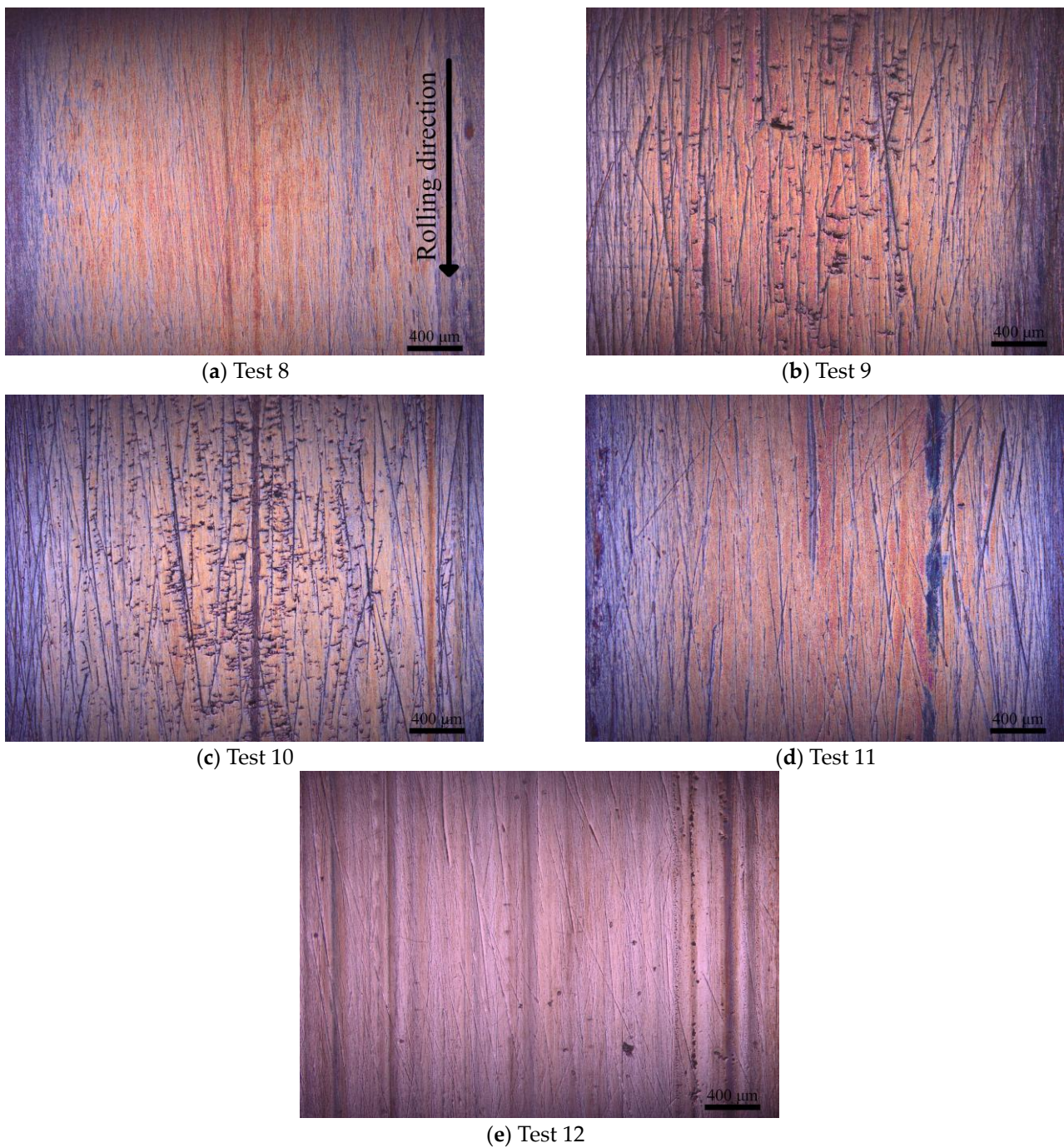


Figure 6. Surface images of the 26 mm discs for (a) Test 8, (b) Test 9, (c) Test 10, (d) Test 11 and (e) Test 12. The arrow indicates the rolling direction for all the images, and the scale bar at the bottom right of the images shows 400 μm .

Test 10 was performed under a lower lambda value of 0.44 and lasted for nearly 15 h with severe pits appearing on the surface (see Figures 6c and 7j). This test also shows faint discoloration on the surface. Test 11 was performed under operating conditions similar to those of Tests 5 and 9 but was terminated manually after 15 h to explore the development of the features on the wear track. No surface damage was observed for this test, although visual features similar to those of Test 9 were exhibited. Similarly, Test 12 was performed under operating conditions similar to those of Test 5, but without any SRR, and was terminated manually after a running period of 114 h (nearly 3 times the running time of Test 5). No visible surface features appear to have formed in this test.

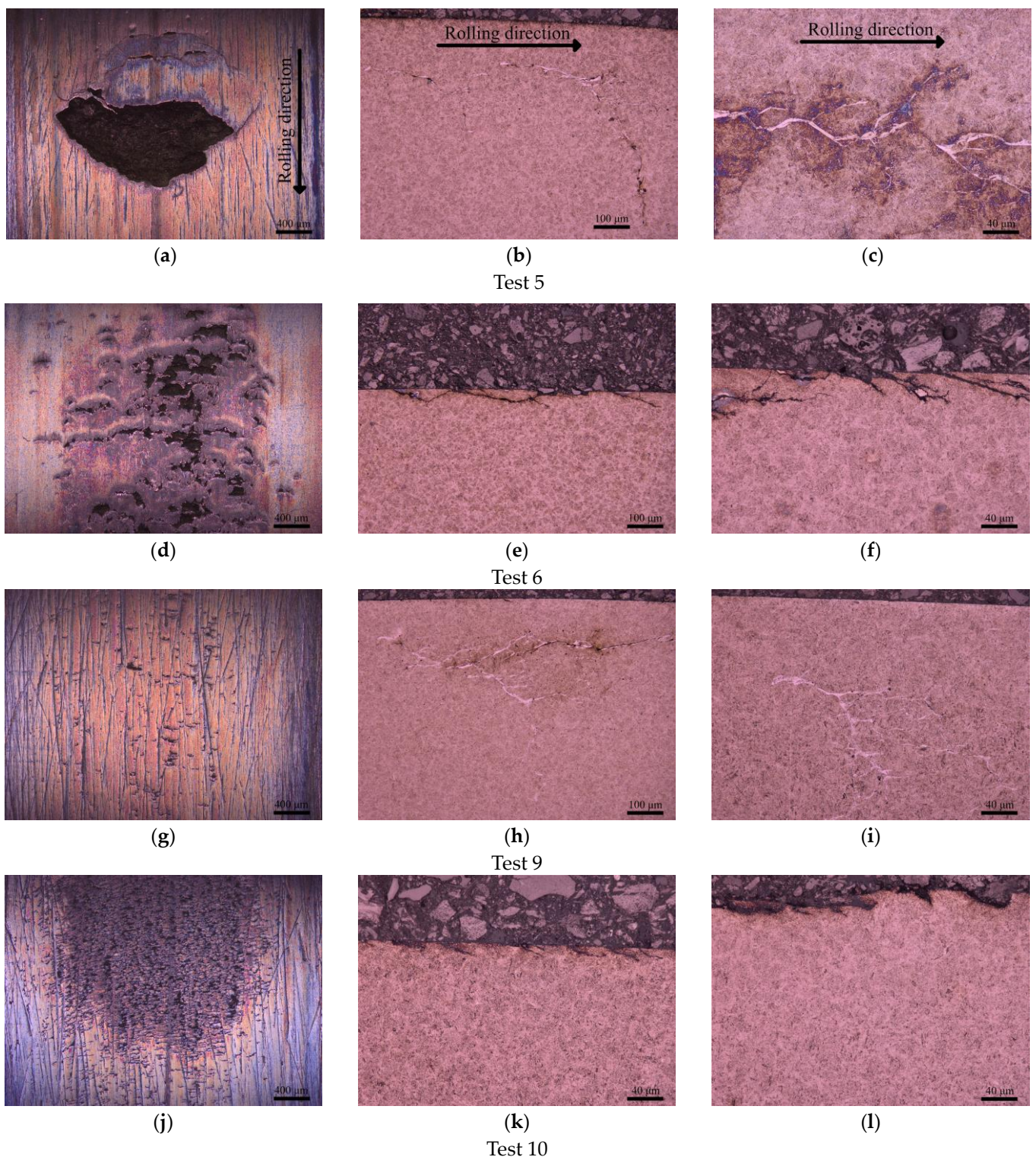


Figure 7. Surface and subsurface analysis for the 26 mm roller is presented in a row for Tests (a–c) 5, (d–f) 6, (g–i) 9 and (j–l) 10. The arrow indicates the rolling direction for all the images in the column. The scale bar for the left column is 400 μm, for the middle column is 100 μm, and for the right column is 40 μm.

3.1.2. Subsurface Analysis of the Failed Samples and Outcome of the Tests

Figure 7 shows the surface damage features and corresponding subsurface analysis using LOM for Tests 5, 6, 9 and 10. The outcomes of the surface and subsurface analysis of the samples are shown in Table 6.

Tests 5, 6 and 10 were automatically shut down due to the vibration amplitude exceeding the threshold as a result of surface damage. As shown, Test 5 failed due to a large spall with a width of 1.9 mm and a length of 0.9 mm. As shown in Figure 7d,j, Tests 6 and 10 failed due to pitting appearing in substantial numbers, mostly concentrated in the centre of the wear track but extending beyond 2 mm in width. Test 9 was manually shut down after over 45 h with a slight increase in vibration level. On the surface of the 26 mm disc, small pits are observed, mostly concentrated in the middle 50% of the wear track.

In Tests 5 and 9, networks of WECs were observed extending over 1 mm in length and depth of the material, and in some cases only 1 mm from each other. In fact, in these tests, only analysing one layer, on average over 10 networks of WECs were identified for each section (see Figure 7i showing one network of WECs). This indicates a substantial density of WECs in the 26 mm roller after a test duration of only 40 to 46 h.

In Tests 6 and 10, several surface-initiated cracks and pits are observed, appearing 30° to 45° degrees from the surface and limited to 200 µm in depth. The cracks appear all around the circumference of the 26 mm roller and lead to surface pitting when reaching an adjacent crack.

3.2. Influence of Operating Parameters on WEC Formation

As lubricant inlet temperature, supply voltage and lambda were shown to be influential in promoting WEC formation (see Table 6), these parameters are investigated statistically in this section.

In analysing the sensor data, the responses during the initial ramping-up period of load and rotational speeds have been eliminated from the analysis in order to focus on those during the steady state. Following this, to capture the response range of each parameter (e.g., lubricant inlet temperature), a quartile method is used to obtain its median, first and third quartiles, and minimum and maximum values. Minimum and maximum are calculated by taking the difference between the third and first quartiles, known as the interquartile range (IQR), multiplying it by 1.5, and subtracting or adding the result to the first quartile or third quartile, respectively.

3.2.1. Range of Temperatures and Lambda in WEC Tests

Due to constant operating conditions during the tests, the tests experienced an IQR of a maximum of 2 °C, and for median temperature below 90 °C, no failures are observed. For temperatures above 90 °C, micropitting, WECs and tests with no damage are observed. In fact, for the tests without any damage, the running time extended beyond 6 times (see Test 4 compared to Tests 5 and 9) and 20 times (see Test 4 compared to Tests 6 and 10) the running times for WEC and micropitting tests, respectively. Thus, lubricant inlet temperature cannot be the only influencer promoting the formation of WECs.

In all the tests, the IQR for lambda was limited to 0.3, which indicates a very small change in lambda within each test. For Tests 1–4, the median lambda is above 4 and no failure is observed. In addition, Test 8 with a lambda of 1.34 and a running time of 35.69 h did not show any failure (see Table 7).

Reducing lambda below 1 resulted in WECs and severe micropitting failures. Under a median lambda of 0.40–0.44 (boundary regime), the discs failed to reach a running time beyond 14.52 h. Tests 5 and 9 show a median lambda of 0.71–0.76, and both failed due to WEC formation at approximately 40 and 46 h. Tests 7, 11 and 12 also present a similar median lambda of 0.71–0.95 but did not fail. For Test 7, no supply voltage was supplied to the discs, and no failure was observed after a running time of 239.71 h. Test 12 was performed without any SRR and, similarly, did not show any failure after a running time of 114.85 h. Test 11 was performed under operating conditions similar to those of Tests 5 and

9 (with a supply voltage of 15 V and an SRR of 15%) but was manually terminated after a short running time of approximately 15 h with no failure.

Table 7. The analysis of the voltage across the discs for the tests. The highlighted cells indicate the main parameters that were changed between the tests.

Test Number	Running Time (h)	Minimum (V)	First Quartile (V)	Median (V)	Third Quartile (V)	Maximum (V)	Failure Type
Test 1	335.77	0.18	0.32	0.38	0.42	0.56	No failure
Test 2	305.38	−0.48	0.45	0.60	1.08	2.02	No failure
Test 3	285.08	0.37	0.64	0.72	0.82	1.10	No failure
Test 4	305.86	0.19	0.79	0.96	1.19	1.79	No failure
Test 5	39.82	1.83	2.71	3.00	3.30	4.18	WECs
Test 6	2.75	0.15	0.41	0.52	0.59	0.85	Other
Test 7	239.71	0.00	0.00	0.00	0.00	0.00	No failure
Test 8	35.69	0.90	1.38	1.55	1.69	2.17	No failure
Test 9	45.72	0.90	2.43	2.95	3.45	4.97	WECs
Test 10	14.52	1.45	1.71	1.82	1.89	2.15	Other
Test 11	14.93	1.51	2.46	2.79	3.09	4.04	No failure
Test 12	114.85	0.15	0.34	0.39	0.46	0.65	No failure

3.2.2. Range of Voltage across the Discs in WEC Tests

This section analyses the voltage across the discs' contact (VADC) to explore if WEC tests show unique characteristics. The quartile analysis of the VADC is detailed in Table 7. For tests without any failure (except Test 11), the median VADC is low and is limited to 1.55 V. For the tests that failed due to severe micropitting, similarly, the median VADC fails to reach beyond 1.82 V. WEC tests show a substantially higher median VADC of 2.95–3.00 V. Similarly, Test 11 also shows a high median VADC of 2.79 V, but due to a low running time of 14.93 h (in comparison to 40–46 h in WEC tests), fails to promote the formation of WECs.

The relationship between lambda and VADC can be shown using the median lambda (see Table 6) and median VADC. Figure 8 shows the median VADC as a function of median lambda for the tests, with labels indicating the test number, median VADC and lambda values for the tests. As can be seen for the lambda values above 4, the VADC reduces to below 1 V.

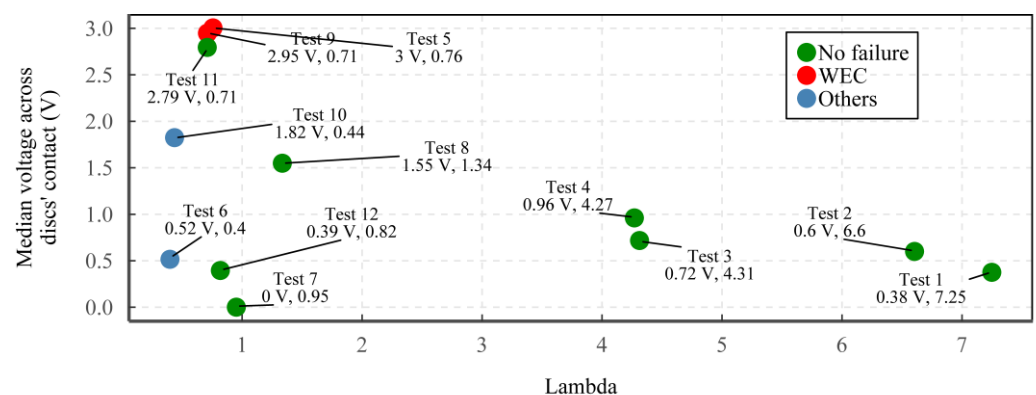


Figure 8. The plot of the median voltage across the discs' contact as a function of median lambda for the tests. Test 11 was stopped at 14.93 h to explore the early initiation of WECs.

However, for lambda values between 0.4 and 1.34 (except Tests 12 and 7 with no slip and no supply voltage, respectively), a curve trend can be seen, with the peak of the trend corresponding to a region of WECs.

With any further decrease in median lambda below this region of WECs, the median VADC reduces substantially, which leads to the severe micropitting region with Tests 6 and 10 failing to reach a running time above 15 h.

Using the illustration, three regions can be realised:

- Region 1 with a median lambda of 0.40–0.44 and a median VADC of 0.52–1.82 V, resulting in severe micropitting.
- Region 2 with a median lambda of 0.71–0.76 and a median VADC of 2.79–3 V, resulting in the formation of WECs.
- Region 3 with a median lambda of 1.34–7.25 and a median VADC of 1.55–0.38 V, showing no failure.

3.2.3. Range of Electric Current, Resistance and Field in WEC Tests

This section analyses the electric current, resistance and electric field in the tests to explore if WEC tests show unique characteristics.

The maximum electric current was limited to 200 μA for the tests. As demonstrated in Table 8, the level of electric current for the WEC tests is lower than that for tests without WECs (except Test 11). For WEC tests, the median electric current ranges from 134.04 to 134.60 μA , compared to 158.67–190.90 μA for non-WEC tests.

Table 8. The analysis of the electric current, resistance and field for the tests. The highlighted cells indicate the main parameters that were changed between the tests.

Test Number	Running Time (h)	Current (μA)		Resistance ($\text{k}\Omega$)		Electric Field (kV/mm)		Normalised Field (V)		Failure Type
		Median	IQR	Median	IQR	Median	IQR	Median	IQR	
Test 1	335.77	190.90	1.31	2.44	0.37	1.36	0.35	0.05	0.02	No failure
Test 2	305.38	185.59	13.64	3.92	4.13	2.38	2.63	0.09	0.10	No failure
Test 3	285.08	183.05	3.25	4.68	0.97	4.37	1.12	0.17	0.04	No failure
Test 4	305.86	177.85	7.26	6.28	2.29	5.93	2.40	0.23	0.09	No failure
Test 5	39.82	134.04	8.18	24.69	4.56	16.65	3.24	3.93	0.77	WECs
Test 6	2.75	187.60	3.51	3.35	1.00	3.27	1.12	1.29	0.44	Other
Test 7	239.71	0.00	0.00	0.00	0.00	0.00	0.00	0.00	0.00	No failure
Test 8	35.69	165.63	5.49	10.43	1.99	9.31	1.88	1.16	0.24	No failure
Test 9	45.72	134.60	21.10	24.36	11.47	18.19	6.18	4.14	1.41	WECs
Test 10	14.52	158.67	2.09	13.08	0.84	11.42	1.13	4.18	0.41	Other
Test 11	14.93	137.16	10.73	22.97	5.67	17.34	3.99	3.94	0.90	No failure
Test 12	114.85	189.97	2.80	2.68	0.79	2.12	0.66	0.48	0.15	No failure

The median electrical resistance of the contact in WEC tests is 24.36–24.69 $\text{k}\Omega$, compared to a maximum of 13.08 $\text{k}\Omega$ for the non-WEC tests (excluding Test 11). This demonstrates that in the WEC tests, the contact demonstrated a substantially greater electrical resistance, which subsequently results in a higher voltage across the contact and a lower electric current through the contact.

Both VADC and the electric current are closely related as they are both related to the electrical behaviour of the discs' contact.

The electric field in this case is determined for the duration of the test by finding the division between the VADC and minimum lubricant film thickness (V/mm). In addition, the division of the VADC and lambda is also calculated in this section and referred to as the "normalised" electric field. This is mainly due to the tests having different initial roughness values and the need to incorporate the influence of roughness. The normalised electric field is in the unit of V but can allow for a better investigation of the electric field, irrespective of the variation in roughness values. As shown in Table 7, the median electric field in WEC tests is 16.65–18.19 kV/mm , compared to a maximum of 11.42 kV/mm for the non-WEC tests (excluding Test 11). This demonstrates that in the WEC tests, the contact demonstrated a substantially greater electric field. It is worth mentioning that for the tests

with no failure, the maximum median electric field is limited to 9.31 kV/mm, which is approximately half of the field experienced for WEC tests. Other no-failure tests such as Tests 1–4 and 12 experienced a median electric field of below 5.93 kV/mm. For the tests failing due to surface-initiated pitting (marked as others), two different median electric fields of 3.27 kV/mm and 11.42 kV/mm are registered; thus, it is not clear if a higher electric field influenced the failures within these two tests. The median normalised electric field in WEC tests is 3.93–4.18 V, compared to a maximum of 1.16 V for the no-failure tests (excluding Test 11). For the tests failing due to surface-initiated pitting (marked as others), despite a lower VADC in comparison to WEC tests, due to a substantially lower lambda, the normalised electric field is 1.29–4.18 V. Especially in the case of Test 10, the normalised electric field shows a greater median normalised electric field than even WEC tests.

3.3. Influence of Roughness on the VADC during the Running-In Period

This section focusses on analysing the VADC for the tests during the initial running-in period to examine if, at this early period, the resistance of the contact differs between WEC and non-WEC tests. The running-in period is defined as the initial stage of the tests, where rotational speed and loads were applied to the discs.

The initial running-in periods for Tests 4, 5, 6, 9 and 11 are analysed in detail; all the tests were performed under approximately the same lubricant inlet temperature of ~95–100 °C, the supply voltage of 15 V, the master shaft speed of 3000 rpm, a radial load of 3340 N and an SRR of 15%, with differences in initial roughness value and lambda between the tests (see Table 5 for the details of the tests). The median lambda for the tests is 4.27, 0.76, 0.4, 0.71 and 0.71, respectively.

As Figure 9c demonstrates, all the tests at the end of the running-in period have only achieved a maximum average VADC of only 0.6 V. Test 4 was conducted under a lambda of 4.27 and shows an increase in average VADC with the increase in the discs' rotating speeds. However, Tests 5, 6, 9 and 11 follow a different trend with no increase in average VADC until reaching 50% of the running-in duration.

Interestingly, for Tests 6, 9 and 11, a sudden increase in the average VADC can be seen beyond 50% of the periods shown in Figure 9; at the end of the period, all VADC values exceed the one observed for Test 4 without any further changes in the rotational speed of the shaft. The running-in occurs over 20 min, which suggests that a substantial increase in average VADC can be achieved in less than 10 min through a change in the electrical resistance of the contact.

However, Test 5, unlike those discussed, stays constant without showing any substantial increase above 0.05 V throughout the running-in period. Nevertheless, as previously discussed, this test also shows a high median VADC for the test (approximately 3 V).

3.4. Electrical Discharges in WEC and Non-WEC Tests

As discussed, for WEC tests, a substantially higher electrical resistance for the contact is observed which resulted in substantially greater VADC. In this section, the electrical discharges within the WEC tests will be studied in detail, with further discussion on their nature, frequency and amplitude across the tests.

3.4.1. Nature of Electrical Discharges in a WEC and a Non-WEC Test

To investigate the nature of electrical discharges, two tests have been selected. Tests 3 and 5 represent two cases with no failure after 285 h and a WEC failure after 38.82 h, respectively. Tests 3 and 5 were performed under the same operating and electrical conditions except for median lambda values of 4.31 and 0.76 and SRR values of 5% and 15%, respectively. The snapshots of ES sensors' signals and VADC at two different points in time are used, which are sufficient for a preliminary analysis of the amplitude and frequency of discharges due to very low fluctuations in the average VADC within each test (see Section 3.2.2).

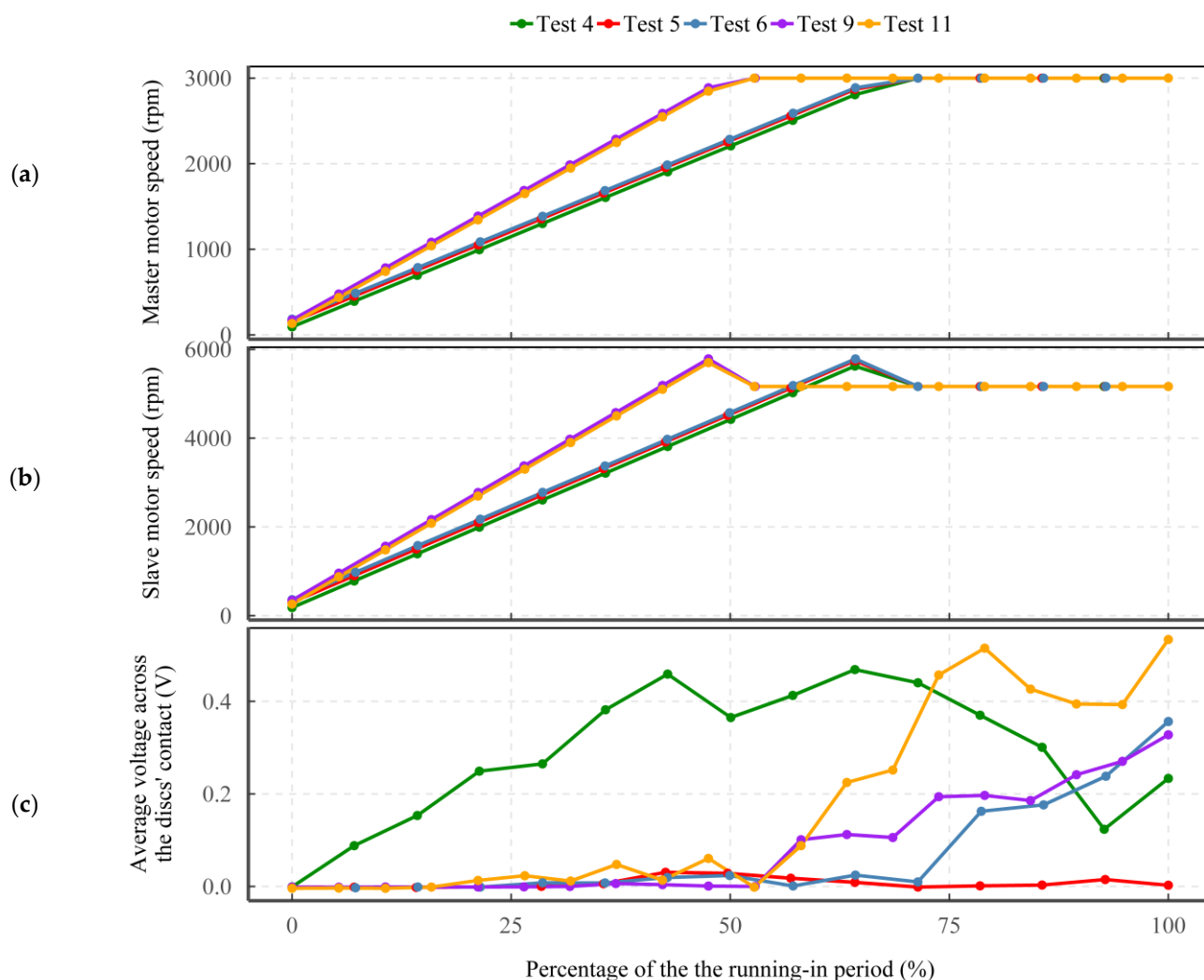


Figure 9. The details of rotational speeds and average VADC during the running-in period for Tests 4, 5, 6, 9 and 11, with (a) master motor shaft speed for the 52 mm disc, (b) slave motor shaft speed for the 26 mm disc and (c) voltage across the discs' contact.

Figure 10 shows the snapshots at 59 h and 245 h of 285 h running time in Test 3, with the ES sensor monitoring the bottom disc and the VADC indicating the presence of multiple overlapping electrical discharges at an amplitude limited to 4 V in VADC and 4 pC in absolute charge. Figure 11 shows the same responses, but for Test 5. As can be seen in the signals from the ES sensor monitoring the bottom disc and the VADC, the amplitude of discharges reaches 5 V in VADC and nearly 5 pC in absolute charge level. In Test 3, only two high-amplitude discharge events are observed in the snapshots, buried between substantial numbers of low-amplitude discharges. However, for Test 5, most of the electrical discharges are of high-amplitude nature lasting over 100 μ s in charging duration, whilst those in Test 3 only reach 50 μ s in duration.

3.4.2. Range of Amplitude and Frequency of Electrical Discharges

As demonstrated by Esmaeili et al. [25], a quantification algorithm developed for analysing the discharges in electrostatic and voltage measurement sensors can be used to quantify the amplitude and number of electrical discharges within the tests. In addition, a quartile analysis is performed for the quantified electrical discharges to statistically characterise the influence of electrical discharges within the tests on WEC formation (see Table 9).

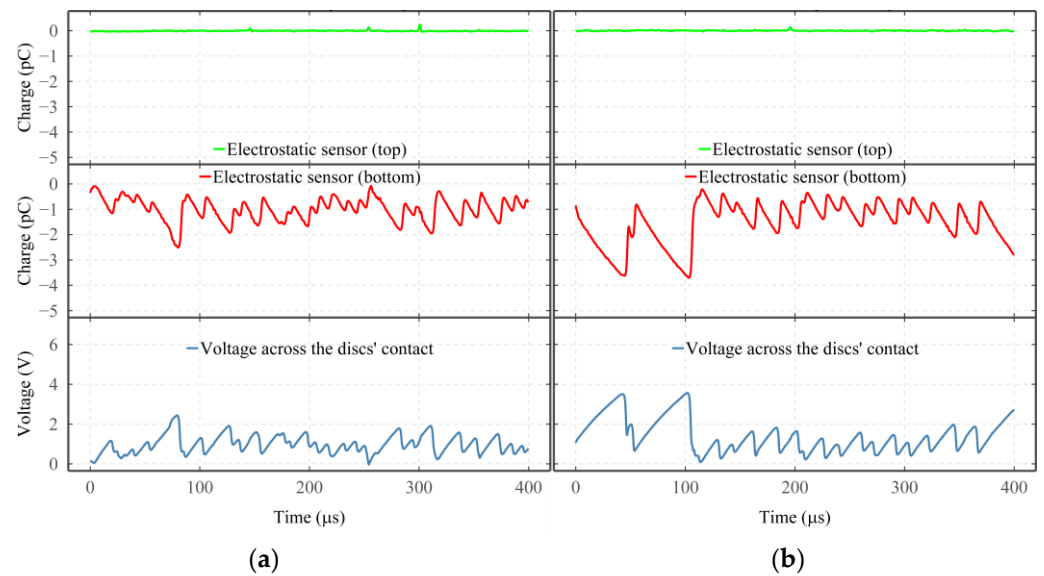


Figure 10. The responses of the ES sensors and VADC captured at (a) 59 h and (b) 245 h of the 285 h running time in Test 3, corresponding to 20% and 86% of the test duration. Operating conditions: rotational speed of 3000 rpm, radial load of 3340 N (maximal contact pressure of 2.5 GPa), supply voltage of 10 V, SRR of 5%, median lambda of 4.31 and median lubricant inlet temperature of 98.5 °C.

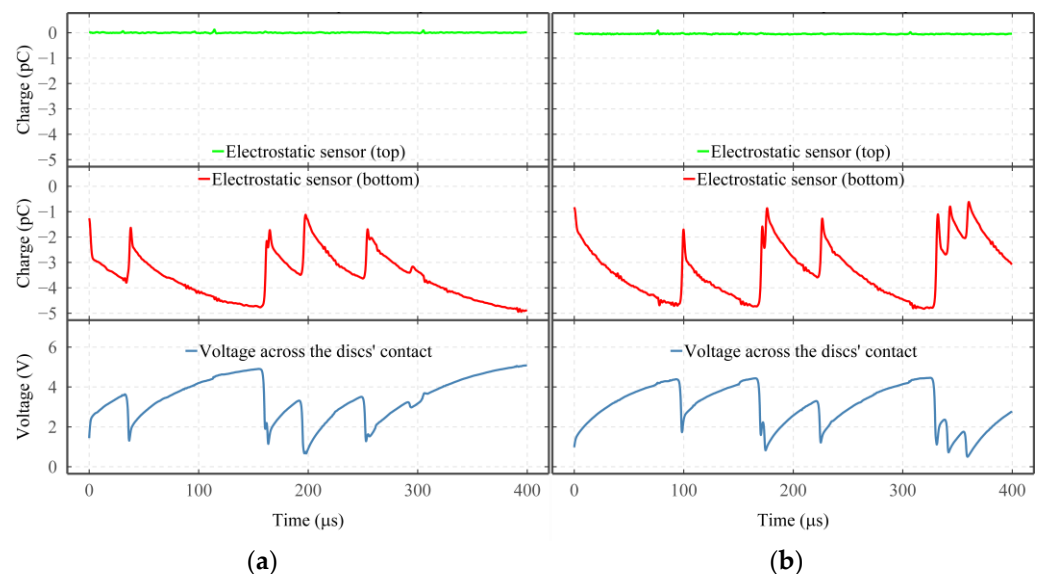


Figure 11. The responses of the ES sensors and VADC captured at (a) 11 h and (b) 39.82 h of the 39.82 h running time in Test 5, corresponding to 28% and 100% of the test duration. Operating conditions: rotational speed of 3000 rpm, radial load of 3340 N (maximal contact pressure of 2.5 GPa), supply voltage of 10 V, SRR of 15%, median lambda of 0.76 and median lubricant inlet temperature of 92.2 °C.

For the tests that did not show any failure (except Test 11), the median discharge amplitude observed for the test ranges from 0.62 to 1.88 V, with the majority of the tests showing a median of approximately 0.6–0.9 V. Tests that failed due to severe pitting show a median voltage of 0.57–1.82 V, which is approximately similar to those of no-failure tests. For the WEC tests (including Test 11), a substantially higher discharge amplitude is observed, with median discharge amplitude ranging from 3.1 to 3.6 V. The IQR of the discharge amplitude also shows a substantially greater range for the tests with WECs, which indicates that despite the presence of high-amplitude electrical discharges, low-amplitude electrical discharges with a first quartile of 2 V also continue to exist within

the tests. On the other hand, for Tests 1–4, 6, 8, 10 and 12, the low IQR indicates that all discharges are of approximately the same amplitude.

Table 9. The analysis of the number and amplitude of discharges for the tests. The highlighted cells indicate the main parameters that were changed between the tests.

Test Number	Running Time (h)	Number of Discharges		Amplitude of Discharges (V)		Failure Type
		Median	IQR	Median	IQR	
Test 1	335.77	37,900	10,500	0.62	0.62	No failure
Test 2	305.38	86,500	18,100	0.87	0.57	No failure
Test 3	285.08	79,900	9000	0.88	0.41	No failure
Test 4	305.86	71,900	20,000	1.06	0.6	No failure
Test 5	39.82	31,300	7225	3.6	3.16	WECs
Test 6	2.75	69,700	5250	0.57	0.63	Other
Test 7	239.71	0	0	0	0	No failure
Test 8	35.69	44,800	10,800	1.88	1	No failure
Test 9	45.72	54,500	27,800	3.21	2.61	WECs
Test 10	14.52	37,100	3600	1.82	1.53	Other
Test 11	14.93	34,800	5200	3.1	3.26	No failure
Test 12	114.85	46,400	8700	0.66	0.55	No failure

Tests 2–4, which did not fail, show the highest median number of electrical discharges. Tests 6 and 9, which failed due to severe micropitting and WEC formation, respectively, show a relatively high number of electrical discharges with a median ranging from 54,500 to 69,700. For Tests 5 and 11 (performed in WEC-critical operating condition), the median number of discharges is 31,300–34,800, which is well below half of the discharges detected in Tests 2–4. Moreover, the IQR shows how the number of electrical discharges detected varied within the tests, with all except Tests 2, 4 and 9 showing relatively small IQR and variation in the number of discharges within the test.

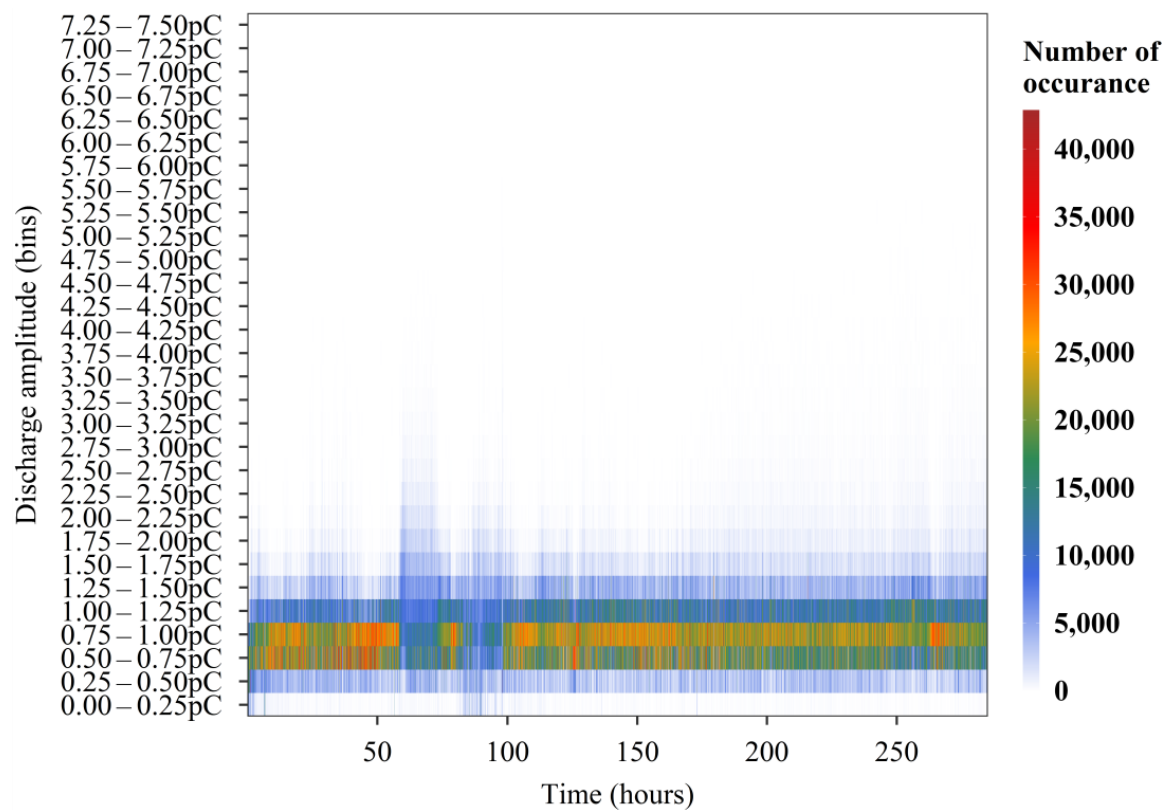
3.5. Detection, Tracking and Classification of Electrical Discharges

3.5.1. Nature of Electrical Discharges in a WEC and a Non-WEC Test

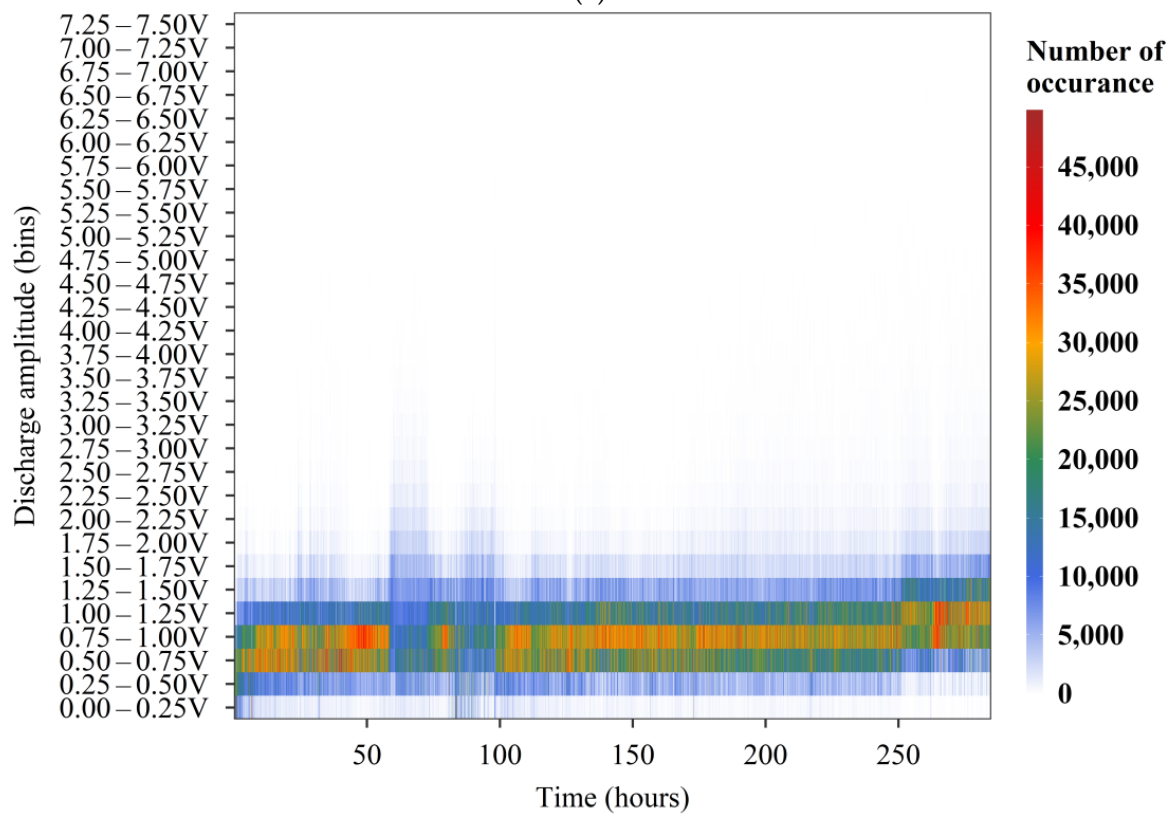
Figures 12 and 13 show the colourmaps of the quantified discharges for Tests 3 and 5, a non-WEC and a WEC test, respectively.

For each test, discharges are both quantified in the signals from the ES sensor monitoring the bottom disc and VADC. The maximum discharge amplitude is limited to 7.5 V and 7.5 pC, so all the colourmaps are limited to 7.5 V and 7.5 pC so a comparison between the two tests can be made.

As shown in Figure 12a, the discharges in Test 3 are more frequent in the discharge strength of 0.5 to 1 pC. Other active discharge strength bins are 0.25–0.5 pC and 1 to 1.50 pC. From approximately 60 to 100 h, an increase in the discharge strength can be observed, active to a discharge bin as high as 3–3.25 pC but appearing less frequent and diminishing after only a few hours. Electrical discharges for Test 5, unlike Test 3, are of substantially higher strength and frequently reach 5.5 pC in discharge amplitude. As shown in Figure 13a, although the discharges are less frequent, they reach a maximum discharge strength of 7.5 pC. These discharges initially are relatively low in amplitude, reaching 1.5 pC at around 2 h. However, they increase to 4.5 pC at around 3.5 h. Two periods are distinguishable in the ES sensor's signals: periods starting at 26 and 33 h, both lasting approximately 2 h, during which the maximum discharge amplitude increases from 6 to 7.5 pC and beyond.



(a)



(b)

Figure 12. Quantified discharges according to their discharge amplitude and their occurrences in Test 3 in the signals from (a) ES sensor monitoring the bottom disc and (b) voltage across discs' contact.

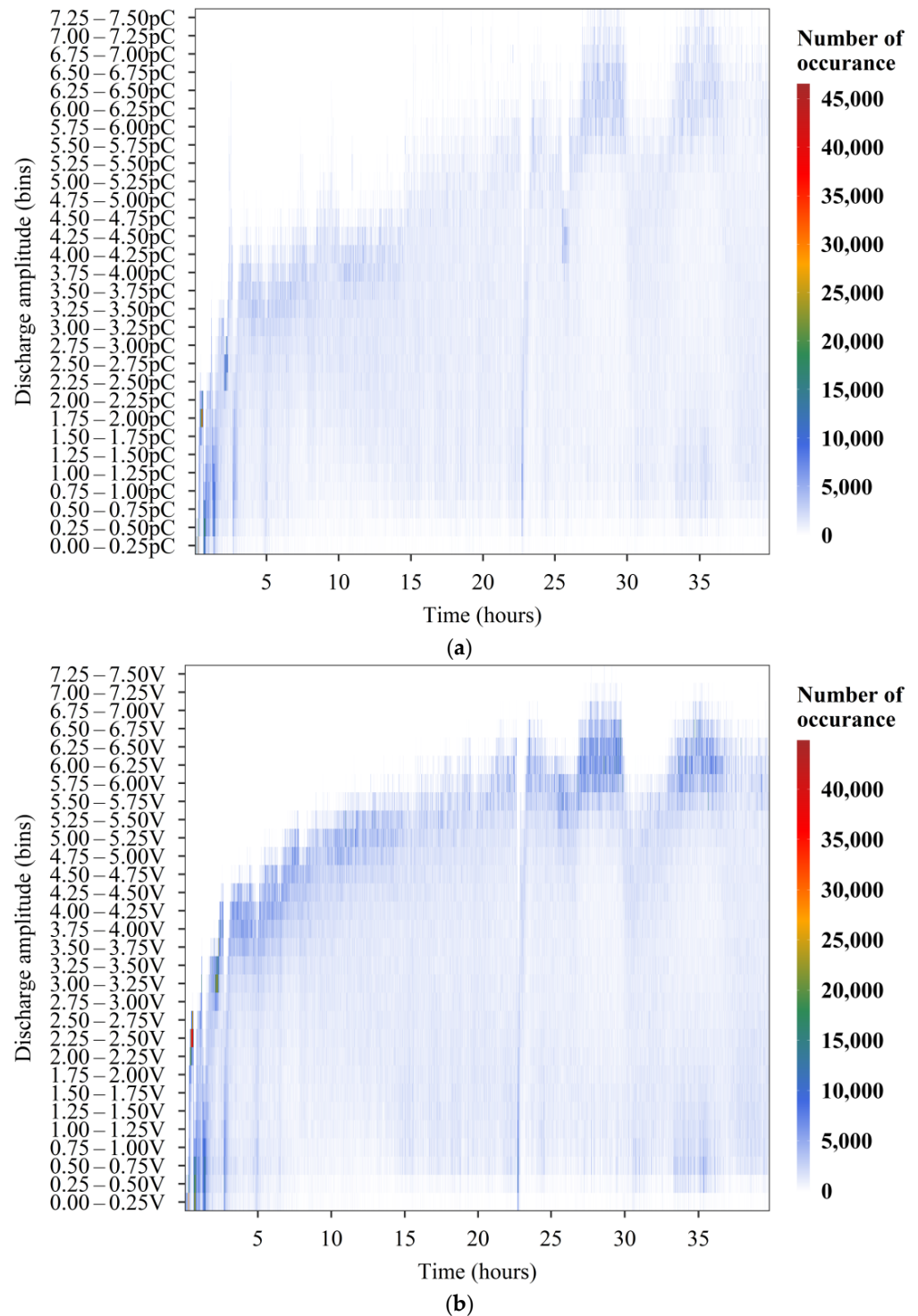


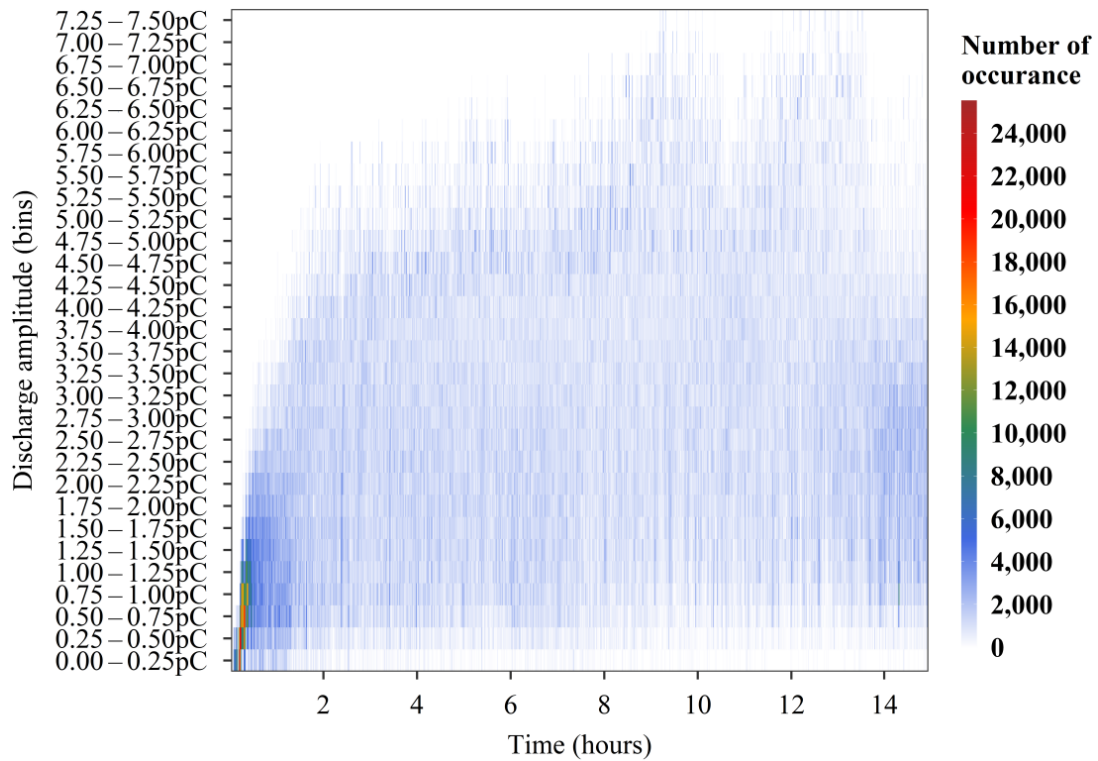
Figure 13. Quantified discharges according to their discharge amplitude and their occurrences in Test 5 in the signals from (a) ES sensor monitoring the bottom disc and (b) voltage across discs' contact.

3.5.2. Early Detection of WEC Critical Condition Using ES Sensing Technique

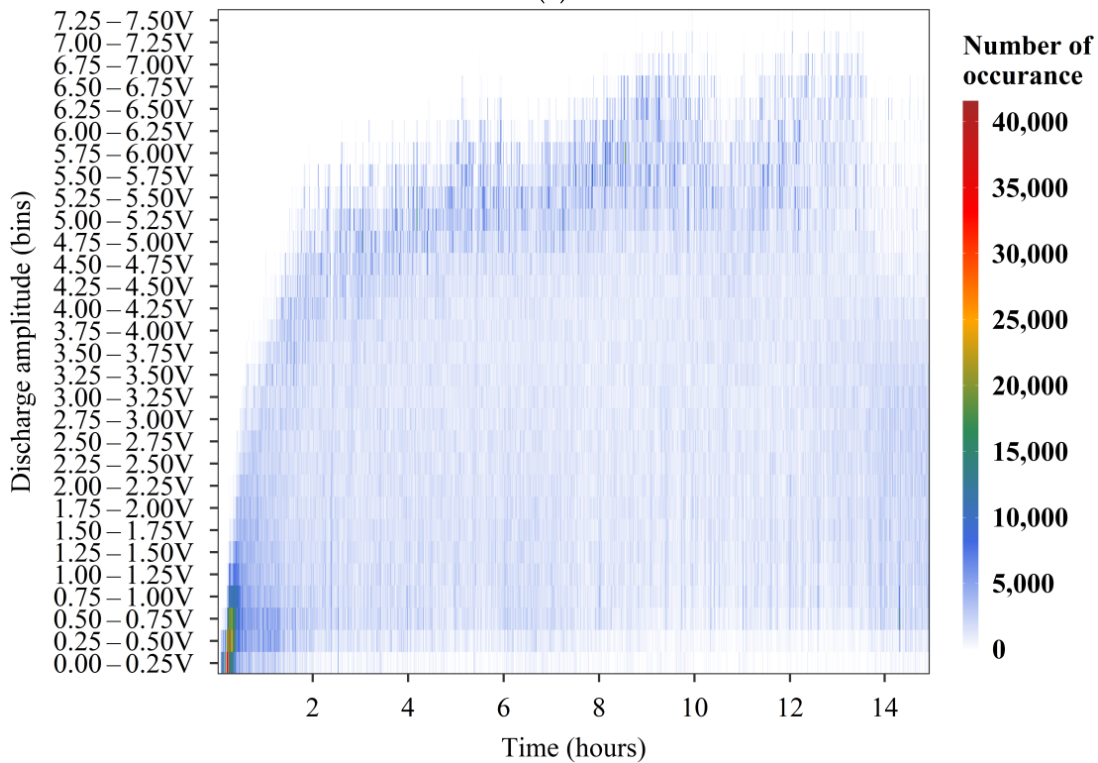
Test 11, a replication of Tests 5 and 9, a WEC test, was conducted with a manual shutdown at 15 h to investigate if WECs are induced in the discs as soon as high-amplitude discharges are observed.

Figure 14 shows the colourmaps for the quantified discharges in the test. As shown, discharges in the signals from both the ES sensor and VADC are of high amplitudes, reaching 7.5 pC and 7.25 V in discharge strength towards the end of the 15 h runtime. The

number of occurrences is also around 4000 discharges per second, which correlates with the discharges detected in the ES sensor's signals at approximately 15 h in Test 5.



(a)



(b)

Figure 14. Quantified discharges according to their discharge amplitude and their occurrences in Test 11 in the signals from (a) ES sensor monitoring the bottom disc and (b) voltage across discs' contact.

Considering this test did not indicate any WEC formation or any surface damage, detection, characterisation and tracking of electrical discharges within the tests can enable the detection of critical discharge levels for WEC formation.

4. Discussion

4.1. Influence of Operating Conditions on WEC Formation

For the WEC tests, it was shown that a median lambda of 0.71–0.76, a median lubricant temperature of 92–97.5 °C, a supply voltage of 10 V and an SRR of 15% are required, whilst if any of these parameters are amended (in case of lambda and lubricant inlet temperature) or removed (in case of the supply voltage and SRR), no WECs will be created. Other factors which were constant across all the tests are a maximal contact pressure of 2.5 GPa and a master shaft speed of 3000 rpm.

High SRR influences the contact by increasing the experienced friction and the disc's temperature, as well as possibly influencing the formation of a tribofilm.

Low lambda (in boundary regime) results in a higher metal-to-metal contact and an increase in friction, which can increase the discs' temperature and lead to a higher rate of tribofilm formation.

High lubricant inlet temperature results in higher contact and discs' temperatures and increases the rate of tribofilm formation. These findings also correlate with the findings in Section 3.1.1, where low lambda, high SRR and high lubricant inlet temperature influenced the formation of tribofilm, which appears as dark red colours on the wear track. The wear track features for WEC tests were distinguishable both in consistency and intensity of the colours in comparison to other tests (see Tests 5, 6, 9 and 10 for examples). A similar analysis using LOM was previously performed for different oils, and it was shown that different compositions of tribofilm are formed for the WEC and non-WEC tests [33]. However, this visual evidence can also be a secondary influence, where the main parameters influencing WEC formation are not the formation of the tribofilm but the existence of high friction, high loading and high electrical inputs.

4.2. Electrical Properties of the Contact

WEC tests showed a substantially high median VADC of 2.95–3.00 V whilst non-WEC tests failed to reach beyond 1.82 V. WEC tests also showed a lower median electric current of 134.04–134.60 μA in comparison to 158.67–190.90 μA for non-WEC tests. Recalling the contact area of 2 mm² for all the tests, WEC tests also showed a lower median current density of 67.02–67.3 $\mu\text{A}/\text{mm}^2$ in comparison to 79.3–95.45 $\mu\text{A}/\text{mm}^2$ for non-WEC tests. WEC tests also demonstrated an electrical resistance of 24.36–24.69 k Ω , compared to a maximum of 13.08 k Ω for the non-WEC tests. WEC tests also showed a high electric field of 16.65–18.19 kV/mm, compared to a maximum of 11.42 kV/mm for the non-WEC tests.

The parameters are all interconnected as high electrical resistance leads to a low electric current through the discs, high VADC and high electric field. This is due to the fact that the electrical circuit is only affected by the resistance of the contact, and when a higher contact resistance is present, the overall resistance of the circuit (resistance of the contact in series with a regulating resistor of 50 k Ω) increases (and with a constant supply voltage of 10 V), which leads to a lower electric current. As the electrical resistance of the contact is current-dependent [11], a lower electric current can also lead to a higher electrical resistance of the contact. This correlates with the findings from Loos et al. [11] and Zuercher et al. [21], where lower electric current resulted in a higher voltage across the contact, higher electric field and accelerated WEC test scenarios. Despite the differences in the operating conditions between the studies by Loos et al. [11], Zuercher et al. [21] and the study presented here, similar electrical properties (i.e., high electrical resistance, high voltage across the contact and low electric current) have been shown to be present in WEC tests.

All the main parameters that were shown to directly or indirectly influence WEC formation (including lambda, lubricant inlet temperature and SRR) also influenced the electrical resistance of the contact. These can lead to abrasive wear and adhesive wear at

the contact due to the presence of a high electrical field and subsequently lead to entries at the surface for the formation of WECs. However, WECs can also be influenced by the high-amplitude electrical discharges interacting with the material inhomogeneities and causing local thermal stress in the subsurface of the material [23].

One interesting observation in this study is that despite a substantially greater λ in Tests 1–4 compared to Tests 5 and 9 (see Section 3.2.1), a lower electrical resistance is observed, which contradicts both the findings by Esmaili et al. [25] and the electrical resistance model of a contact presented by Loos et al. [11]. One possible explanation might be the influence of an additive (i.e., tribofilm formation), which can lead to the formation of layers that provide electrical resistance [34,35] (see Figure 15). These “layers” can be in the form of a tribofilm and/or clusters formed due to molecular interactions [5], which both can increase the electrical resistance. In a study by Judith Züllich [27] on an IPAT bearing test rig, a variety of lubricants with different compositions of VISCOPLEX6-054 (PMMA) and zinc dithiophosphate, under identical operating conditions, were used, and none of the lubricants, containing only PAO-8, PAO-8 and zinc dithiophosphate, and PAO-8 and VISCOPLEX6-054 (PMMA), showed a voltage of greater than 4 V (1 V per contact). However, the lubricant with a mixture of PAO-8, VISCOPLEX6-054 (PMMA) and zinc dithiophosphate showed a voltage of greater than 10 V (2.5 V per contact) and failed due to WEC formation. It was argued that a mixture of PMMA influences the chain length of layered structure from ZnDPP by reducing the chain length of the compounds and allowing for the formation of the tribolayers at lower ZnDDP concentrations. PMMA enables the formation of ZnS-line compounds as well as short-chain polyphosphates and zinc polyphosphates, in contrast to the ZnDDP layers (without PMMA) which are free of sulfur [36–38].

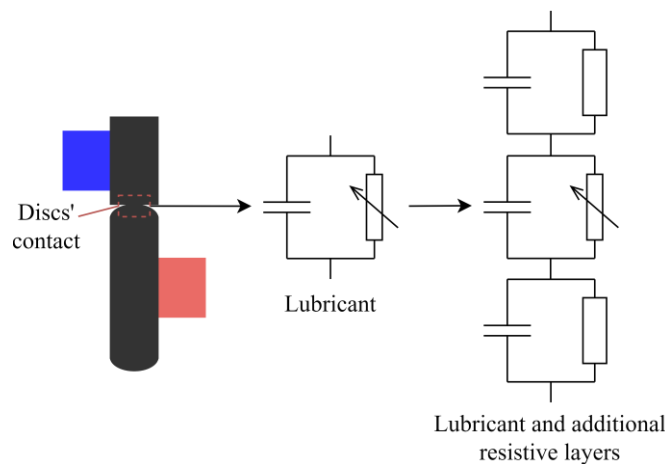


Figure 15. The electrical resistance of the contact with lubricant, and lubricant and resistive layers.

In these cases, the overall resistance of the contact will be a combination of the resistance of the formed layers and the lubricant (see Figure 15).

As the running-in period takes over 20 min and is a dynamic load and speed case with minimal tribofilm formation, this allowed the investigation of the contact’s electrical model to assess if the electrical circuit is somewhat similar to the one described by Esmaili et al. [25] but influenced by the tribofilm formation, or if completely different electrical models exist in these cases. Comparing the tests presented in Section 3.3, it can be realised that the majority of the tests, during the running-in period, follow the electrical behaviour discussed by Esmaili et al. [25], where lower λ leads to a lower VADC. However, it was found that the average VADC rapidly increases for the tests with a low λ towards the end of the running-in period, possibly due to the mechanisms discussed here.

4.3. Electrical Discharges within the Tests

The nature of electrical discharges in the WEC tests is substantially different from the nature of those in the non-WEC tests. The electrical discharges in the WEC tests have a higher amplitude, longer charging duration and appear less frequently. These high-amplitude discharges are influenced by the high electrical resistance of the contact, which permits the building up of charges at the contact and high-intensity discharge events. The statistical analysis of electrical discharges further confirmed the results obtained, where a higher electrical resistance of the contact was observed in WEC tests.

As the supply voltage is kept constant across these tests, the charging rate is also constant, which leads to a longer charging period in WEC tests (see Section 3.4.1 for a comparison of the charging period between WEC and non-WEC tests). Subsequently, longer charging periods result in a lower number of electrical discharges. However, even for the WEC tests, due to the frequent metal-to-metal contacts at low λ , high-amplitude electrical discharges are often accompanied by those of lower amplitudes (see Section 3.4.1 and the IQR for WEC tests in Table 9). The findings here also confirm the results obtained by Zuercher et al. [21] and Loos et al. [11], where lower electric currents (higher electrical resistance and average voltage across the bearings) were shown to promote the formation of WECs, despite the higher number of electrical discharges at higher electric current.

As the high-amplitude electrical discharges cause the formation of WECs, it can be argued that the presence of lower-amplitude electrical discharges in a test can assist in prolonging the life and delaying the formation of WECs, as these discharges prevent the presence of high-amplitude discharges by releasing the charges across the contact. These high-amplitude discharges (together with a high electric field) were previously suggested to result in the formation of WECs by promoting the tribochemical and electrochemical reactions on the nascent surfaces [11] and/or lead to thermal heating within the material and the formation of WECs [23]. Thus, if the intensity of these discharges is monitored, the conditions that can lead to WEC formation can be detected, which can lead to early detection of WECs.

4.4. Early Detection of WEC Critical Discharges Using Electrostatic Sensing Technique

A comparison of Figures 12 and 13 shows that the frequency of discharges in WEC tests and within a discharge bin was limited to approximately 10,000 discharges per second, whilst this was much greater for a non-WEC test at approximately 25,000. This can suggest that the low-amplitude discharges, although 2.5 times more frequent, are not as detrimental as those less repetitive but much higher in discharge amplitude. Test 11 was performed with a short running time of only 15 h, and despite showing electrical behaviour similar to that seen in Tests 5 and 9, and being performed in similar operating conditions, no WECs were found in the subsurface analysis of the discs. This can indicate that the WECs are formed at some point between 15 and 50 h of running time in Tests 5 and 9 and that monitoring the discharges using ES and/or VADC can provide early information on the condition that can lead to WEC formation. This is further reinforced by the fact that for Tests 5 and 9, the population of the WECs was extremely dense, meaning that these operating conditions were extremely critical for WEC formation.

However, the exact initiation and propagation stages of WECs in these tests are not exactly clear, and even at periods where no WECs were found, there could be microcracks formed that are difficult to detect under LOM. Nevertheless, this technique can be used to provide the earliest signatures of potential WEC damage in an electrical environment, not by monitoring the degradation signatures of the discs, but by evaluating the conditions and the electrical discharges that can lead to WEC formation.

4.5. Limitations of the Study

The limitations of the current study are summarised as follows:

- The exact ranges of SRR, supply voltage, load, maximal contact pressure, and lubricant and contact temperatures are not fully studied to characterise how different values

accelerate or decelerate the formation of WECs. In addition, a current source can allow the investigation of the level of electric current and the resistance of the contact, as well as its influence on WEC formation.

- No detailed tribofilm analysis was performed in this study, so only a visual comparison was given. Further tribofilm analysis needs to be performed for WEC and non-WEC tests to explore the similarities and differences.
- Only one lubricant was used in this study, with different additive packages that all can influence the electrical behaviour of the contact under different contact conditions. Thus, a variety of lubricants, including PAO without any additives, should be used to investigate the underlying mechanism(s) behind the high electrical resistance of the contact.
- In the study performed here, the ES sensors were purposefully positioned at the inlet of the discs' contact to have little interaction with the lubricant, debris and particles emitted due to material degradation. As a result, no detailed analysis of the signatures associated with the material degradation event in ES sensors was performed.

5. Conclusions

This study has focussed on investigating the influence of electrical discharges in an oil-lubricated rolling contact under low-current-density conditions. Tests under a variety of temperature, lambda and SRR conditions were performed on a TE74 twin-roller test rig to study the influence of these parameters on the electrical discharges and their combined influence, together with the electrical discharges, on WEC formation. Following this, ES and voltage monitoring techniques, having shown capabilities in the detection of electrical discharges, were utilised to detect and diagnose WEC formation in the discs. The main conclusions from this study are as follows:

- Operating parameters such as oil temperature, lambda and SRR all influence the average VADC. An increase in oil inlet temperature results in an increase in the average VADC, whilst an increase in SRR substantially increases the average VADC. However, for lambda, there are three distinct regions:
 - Region 1 with a median lambda of 0.4–0.44 and a median VADC of 0.52–1.82 V, resulting in severe micropitting.
 - Region 2 with a median lambda of 0.71–0.76 and a median VADC of 2.79–3 V, resulting in the formation of WECs.
 - Region 3 with a median lambda of 1.34–7.25 and a median VADC of 1.55–0.38 V, showing no failure.
- WEC formation is influenced by lambda, SRR and supply voltage, and this study found that WECs cannot be induced in the discs without a supply voltage, SRR and a lambda of 0.71 to 0.76.
- Discharging characteristics in a WEC test are found to be different from those in a non-WEC test; i.e., for a WEC test, the discharges are less frequent but appear in high amplitudes, whilst for a non-WEC test, the number of discharges is 2 or 3 times higher but the discharges only reach one-third of the discharge amplitude of those observed in a non-WEC test. This could be used to detect WEC failures using ES sensors.
- As both average VADC and discharges are only influenced by the electrical resistance of the contact, the difference in the electrical behaviour of the non-WEC and WEC tests is possibly due to the formation of electrically resistive tribolayers. However, it is not yet clear what the mechanisms for the formation of WECs under the influence of electrical discharges are.
- The quantification algorithm developed in this study has been shown to be effective in characterising the electrical discharges in both signals from the ES sensors and VADC, and in one study it was shown that WECs can be detected by assessing the conditions that lead to WEC formation, i.e., high-amplitude electrical discharges, before any WECs are formed in the samples. This can substantially improve fault detection and prognosis and be utilised to change the operating conditions to prevent WEC formation.

Author Contributions: Conceptualisation, K.E.; methodology, K.E.; software, K.E.; investigation, K.E.; resources, W.H.; writing—original draft preparation, K.E.; writing—review and editing, L.W., T.J.H., N.M.W. and W.H.; supervision, L.W., T.J.H., N.M.W. and W.H.; project administration, L.W.; funding acquisition, L.W., N.M.W. and W.H. All authors have read and agreed to the published version of the manuscript.

Funding: The authors would like to acknowledge Schaeffler Technologies AG & Co. KG, Germany, for technical support. This research was funded by University of Southampton and Schaeffler Technologies AG & Co. KG.

Data Availability Statement: All data will be made available on request to the corresponding author's email with appropriate justification.

Conflicts of Interest: The authors declare no conflict of interest.

Appendix A

This section is based on [39,40] (pp. 293–336 of [40]). The viscosity of the lubricant is influenced by the temperature and often the lubricant manufacturers report the kinematic viscosity of the lubricant at 40 °C and 100 °C. The kinematic viscosity of the lubricant can then be found by:

$$v_T = \frac{\eta_T}{\rho_{oil}},$$

where v_T is the kinematic viscosity at a temperature T in [m²/s], ρ_{oil} is the density of oil in [kg/m³] and η_T is the dynamic viscosity at temperature T in [Pa.s]. The kinematic viscosity of the lubricant can be estimated using Andrade equation:

$$\eta_T = A e^{\frac{B}{T}},$$

where A and B are Andrade coefficients, and T is the temperature. The Andrade coefficients are defined as follows:

$$B = \frac{\ln \eta_{40} - \ln \eta_{100}}{\frac{1}{T_{40}} - \frac{1}{T_{100}}} \quad A = \eta_{40} e^{-\frac{B}{T_{40}}}.$$

Reduced Young's modulus of the two discs can be calculated in [Pa] using:

$$\frac{1}{E^*} = \frac{1}{2} \left[\frac{1 - \nu_1^2}{E_1} + \frac{1 - \nu_2^2}{E_2} \right],$$

where E_1 and E_2 are the elastic modulus for two discs in [Pa], and ν_1 and ν_2 are the Poisson's ratio for the two discs. The sum of curvature for the two contacting bodies is given in [1/m] as:

$$\sum \rho = \frac{1}{R_x} + \frac{1}{R_y} = \left(\frac{1}{R_{1x}} + \frac{1}{R_{2x}} \right) + \left(\frac{1}{R_{1y}} + \frac{1}{R_{2y}} \right),$$

where R_{1x} and R_{2x} are the radius of the discs in the rolling direction in [m], R_{1y} and R_{2y} are the radius of the discs in the transverse direction in [m], R_x and R_y are the reduced radius of curvature in the rolling and transverse direction in [m], respectively.

Contact dimensions are calculated for the ellipse using the following equations:

$$a = \left(\frac{6\bar{k}^2 \bar{\epsilon} W}{\pi E^* \sum \rho} \right)^{\frac{1}{3}} \quad b = \left(\frac{6\bar{\epsilon} W}{\pi \bar{k} E^* \sum \rho} \right)^{\frac{1}{3}} \quad A = \pi a b.$$

W is the load applied to the discs in [N], \bar{k} is simplified ellipticity parameter and $\bar{\varepsilon}$ is the elliptic integral, defined as:

$$\bar{k} = 1.0339 \left(\frac{R_y}{R_x} \right)^{0.636} \quad \bar{\varepsilon} = 1.0003 + \frac{0.5968 R_x}{R_y}.$$

The maximum contact pressures in [Pa] can thus be calculated using the contact dimensions and the load applied:

$$P_{\max} = \frac{3 W}{2 \pi a b}.$$

U is the entrainment surface velocity of the discs in [m/s]:

$$U = \frac{U_1 + U_2}{2}.$$

k is the ellipticity parameter:

$$k = \frac{a}{b}.$$

The minimum elasto-hydrodynamic film thickness in [m] is defined as:

$$\frac{h_0}{R_x} = 3.63 \left(\frac{U \eta_0}{E^* R_x} \right)^{0.68} (\alpha E^*)^{0.49} \left(\frac{W}{E^* R_x^2} \right)^{-0.073} \left(1 - e^{-0.68 k} \right).$$

α is the pressure-viscosity coefficient in [m²/N], η_0 is the viscosity at atmospheric pressure of the lubricant in [Pa.s]. The lambda value can be calculated using the following equation by considering the RMS roughness of the surfaces for discs in [m]:

$$\lambda = \frac{h_0}{\sqrt{R_{q1}^2 + R_{q2}^2}}.$$

References

- Punga, F.; Hess, W. Eine Erscheinung an Wechsel- und Drehstromgeneratoren. *Elektrotechnik Und Masch.* **1907**, *25*, 615–618.
- Fleischmann, L. Ströme in Lagern und Wellen. *Elektr. Kraftbetriebe Und Bahnen* **1909**, 352–353.
- Alger, P.L.; Samson, H.W. Shaft currents in electric machines. *Trans. Am. Inst. Electr. Eng.* **1924**, *XLIII*, 235–245. [[CrossRef](#)]
- Muetze, A.; Strangas, E.G. On inverter induced bearing currents, bearing maintenance scheduling, and prognosis. In Proceedings of the 2014 International Conference on Electrical Machines (ICEM), Berlin, Germany, 2–5 September 2014; pp. 1915–1921.
- Holweger, W.; Bobbio, L.; Mo, Z.; Fliege, J.; Goerlach, B.; Simon, B. A Validated Computational Study of Lubricants under White Etching Crack Conditions Exposed to Electrical Fields. *Lubricants* **2023**, *11*, 45. [[CrossRef](#)]
- Boyanton, H.E.; Hodges, G. Bearing fluting [motors]. *IEEE Ind. Appl. Mag.* **2002**, *8*, 53–57. [[CrossRef](#)]
- Plazenet, T.; Boileau, T.; Caironi, C.; Nahid-Mobarakeh, B. An overview of shaft voltages and bearing currents in rotating machines. In Proceedings of the 2016 IEEE Industry Applications Society Annual Meeting, Portland, OR, USA, 2–6 October 2016; pp. 1–8.
- Busse, D.; Erdman, J.; Kerkman, R.; Schlegel, D.; Skibinski, G. Characteristics of shaft voltage and bearing currents. *IEEE Ind. Appl. Mag.* **1997**, *3*, 21–32. [[CrossRef](#)]
- Zuercher, M.; Heinzler, V.; Schlücker, E.; Esmaeili, K.; Harvey, T.J.J.; Holweger, W.; Wang, L. Early failure detection for bearings in electrical environments. *Int. J. Cond. Monit.* **2018**, *8*, 24–29. [[CrossRef](#)]
- Esmaeili, K.; Zuercher, M.; Wang, L.; Harvey, T.; Holweger, W.; White, N.; Schlücker, E. A study of white etching crack bearing failure detection using electrostatic sensing in wind turbine gearboxes. *Int. J. Cond. Monit.* **2018**, *8*, 82–88. [[CrossRef](#)]
- Loos, J.; Bergmann, I.; Goss, M. Influence of currents from electrostatic charges on WEC formation in rolling bearings. *Tribol. Trans.* **2015**, *59*, 865–875. [[CrossRef](#)]
- Richardson, A.D.; Evans, M.-H.; Wang, L.; Wood, R.J.K.; Ingram, M.; Meuth, B. The Evolution of White Etching Cracks (WECs) in Rolling Contact Fatigue-Tested 100Cr6 Steel. *Tribol. Lett.* **2018**, *66*, 6. [[CrossRef](#)]
- Evans, M.-H.; Richardson, A.D.; Wang, L.; Wood, R.J.K.; Anderson, W.B. Confirming subsurface initiation at non-metallic inclusions as one mechanism for white etching crack (WEC) formation. *Tribol. Int.* **2014**, *75*, 87–97. [[CrossRef](#)]
- Richardson, A.D.; Evans, M.-H.; Wang, L.; Wood, R.; Ingram, M. Thermal desorption analysis of hydrogen in non-hydrogen-charged rolling contact fatigue-tested 100Cr6 steel. *Tribol. Lett.* **2018**, *66*, 4. [[CrossRef](#)] [[PubMed](#)]

15. Lund, T.B. Sub-surface initiated rolling contact fatigue—Influence of non-metallic inclusions, processing history, and operating conditions. *J. ASTM Int.* **2010**, *7*, 1–12. [[CrossRef](#)]
16. Grabulov, A.; Ziese, B.; Zandbergen, H.W. TEM/SEM investigation of microstructural changes within the white etching area under rolling contact fatigue and 3-D crack reconstruction by focused ion beam. *Scr. Mater.* **2007**, *57*, 635–638. [[CrossRef](#)]
17. Becker, C.P. Microstructural Changes Around Non-Metallic Inclusions Caused by Rolling Contact Fatigue of Ball-bearing Steels. *Met. Technol.* **1981**, *8*, 234–243. [[CrossRef](#)]
18. Šmeļova, V.; Schwedt, A.; Wang, L.; Holweger, W.; Mayer, J. Electron microscopy investigations of microstructural alterations due to classical rolling contact fatigue (RCF) in martensitic AISI 52100 bearing steel. *Int. J. Fatigue* **2017**, *98*, 142–154. [[CrossRef](#)]
19. Šmeļova, V.; Schwedt, A.; Wang, L.; Holweger, W.; Mayer, J. Microstructural changes in White Etching Cracks (WECs) and their relationship with those in Dark Etching Region (DER) and White Etching Bands (WEBs) due to Rolling Contact Fatigue (RCF). *Int. J. Fatigue* **2017**, *100*, 148–158. [[CrossRef](#)]
20. Wranik, J.; Holweger, W.; Lutz, T.; Albrecht, P.; Reichel, B.; Wang, L. A Study on Decisive Early Stages in White Etching Crack Formation Induced by Lubrication. *Lubricants* **2022**, *10*, 96. [[CrossRef](#)]
21. Zuercher, M. *Influence of Operating Parameters on WEC Formation*; University of Southampton: Southampton, UK, 2016; pp. 1–30.
22. Loos, J.; Bergmann, I.; Goss, M. Influence of High Electrical Currents on WEC Formation in Rolling Bearings. *Tribol. Trans.* **2021**, *64*, 708–720. [[CrossRef](#)]
23. Holweger, W.; Wolf, M.; Merk, D.; Blass, T.; Goss, M.; Loos, J.; Barteldes, S.; Jakovics, A. White etching crack root cause investigations. *Tribol. Trans.* **2015**, *58*, 59–69. [[CrossRef](#)]
24. Spille, J.; Wranik, J.; Barteldes, S.; Mayer, J.; Schwedt, A.; Zürcher, M.; Lutz, T.; Wang, L.; Holweger, W. A study on the initiation processes of white etching cracks (WECs) in AISI 52100 bearing steel. *Wear* **2021**, *477*, 203864. [[CrossRef](#)]
25. Esmaeili, K.; Wang, L.; Harvey, T.J.; White, N.M.; Holweger, W. Electrical Discharges in Oil-Lubricated Rolling Contacts and Their Detection Using Electrostatic Sensing Technique. *Sensors* **2022**, *22*, 392. [[CrossRef](#)] [[PubMed](#)]
26. ASTM 52100 Bearing Steel. Available online: <http://www.astmsteel.com/product/52100-bearing-steel-aisi/> (accessed on 5 December 2020).
27. Züllich, J. Untersuchungen zur Entstehung von White Etching Cracks in Kugellagern im Zusammenhang mit der Additivierung von Schmierstoffen. Master's Thesis, Friedrich-Alexander-Universität Erlangen-Nürnberg, Erlangen, Germany, 2016.
28. Steinweg, F.; Mikitisin, A.; Oezel, M.; Schwedt, A.; Janitzky, T.; Hallstedt, B.; Broeckmann, C.; Mayer, J. Formation of White Etching Cracks under electrical current flow—Influence of load, slip and polarity. *Wear* **2022**, *504–505*, 204394. [[CrossRef](#)]
29. Dogahe, K.J.; Guski, V.; Mlikota, M.; Schmauder, S.; Holweger, W.; Spille, J.; Mayer, J.; Schwedt, A.; Görlach, B.; Wranik, J. Simulation of the Fatigue Crack Initiation in SAE 52100 Martensitic Hardened Bearing Steel during Rolling Contact. *Lubricants* **2022**, *10*, 62. [[CrossRef](#)]
30. Gould, B.; Demas, N.; Erck, R.; Lorenzo-Martin, M.C.; Ajayi, O.; Greco, A. The effect of electrical current on premature failures and microstructural degradation in bearing steel. *Int. J. Fatigue* **2021**, *145*, 106078. [[CrossRef](#)]
31. Gould, B.; Demas, N.G.; Pollard, G.; Jelita Rydel, J.; Ingram, M.; Greco, A.C. The effect of lubricant composition on white etching crack failures. *Tribol. Lett.* **2019**, *67*, 7. [[CrossRef](#)]
32. Shimizu, Y.; Spikes, H.A. The influence of slide–roll ratio on ZDDP tribofilm formation. *Tribol. Lett.* **2016**, *64*, 19. [[CrossRef](#)]
33. Ruellan, A.; Stadler, K.; Jelita Rydel, J.; Ryan, H. The influence of lubricant formulation on early thrust and radial bearing damage associated with white etching cracks. *Proc. Inst. Mech. Eng. Part J J. Eng. Tribol.* **2020**, *235*, 1047–1059. [[CrossRef](#)]
34. Spikes, H. The history and mechanisms of ZDDP. *Tribol. Lett.* **2004**, *17*, 469–489. [[CrossRef](#)]
35. Georges, J.M.; Martin, J.M.; Mathia, T.; Kapsa, P.; Meille, G.; Montes, H. Mechanism of boundary lubrication with zinc dithiophosphate. *Wear* **1979**, *53*, 9–34. [[CrossRef](#)]
36. Yamaguchi, E.S.; Zhang, Z.; Kasrai, M.; Bancroft, G.M. Study of the interaction of ZDDP and dispersants using X-ray absorption near edge structure spectroscopy—Part 2: Tribochemical reactions. *Tribol. Lett.* **2003**, *15*, 385–394. [[CrossRef](#)]
37. Zhang, Z.; Kasrai, M.; Bancroft, G.M.; Yamaguchi, E.S. Study of the interaction of ZDDP and dispersants using X-ray absorption near edge structure spectroscopy—Part 1: Thermal chemical reactions. *Tribol. Lett.* **2003**, *15*, 377–384. [[CrossRef](#)]
38. Yin, Z.; Kasrai, M.; Fuller, M.; Bancroft, G.M.; Fyfe, K.; Tan, K.H. Application of soft X-ray absorption spectroscopy in chemical characterization of antiwear films generated by ZDDP—Part I: The effects of physical parameters. *Wear* **1997**, *202*, 172–191. [[CrossRef](#)]
39. Eschmann, P.; Hasbargen, L.; Weigand, K. *Ball and Roller Bearings: Theory, Design, and Application*; John Wiley & Sons: New York, NY, USA, 1985.
40. Stachowiak, G.W.; Batchelor, A.W. *Engineering Tribology*, 4th ed.; Butterworth-Heinemann: Oxford, UK; Elsevier: Amsterdam, The Netherlands, 2013; ISBN 9780123977762.

Disclaimer/Publisher's Note: The statements, opinions and data contained in all publications are solely those of the individual author(s) and contributor(s) and not of MDPI and/or the editor(s). MDPI and/or the editor(s) disclaim responsibility for any injury to people or property resulting from any ideas, methods, instructions or products referred to in the content.